A Numerical Study of the Variability and the Separation of the Gulf Stream, Induced by Surface Atmospheric Forcing and Lateral Boundary Flows

TAL EZER AND GEORGE L. MELLOR

Program in Atmospheric and Oceanic Sciences, Princeton University, Princeton, New Jersey

(Manuscript received 2 July 1991, in final form 7 October 1991)

ABSTRACT

A primitive equation regional model is used to study the effects of surface and lateral forcing on the variability and the climatology of the Gulf Stream system. The model is an eddy-resolving, coastal ocean model that includes thermohaline dynamics and a second-order turbulence closure scheme to provide vertical mixing. The surface forcing consists of wind stress and heat fluxes obtained from the Comprehensive Ocean–Atmosphere Data Set (COADS). Sensitivity studies are performed by driving the model with different forcing (e.g., annual versus zero surface forcing or monthly versus annual forcing). The model climatology, obtained from a five-year simulation of each case, is then compared to observed climatologies obtained from satellite-derived SST and hydrocast data.

The experiments in which surface heat flux and wind stress were neglected show less realistic Gulf Stream separation and variability, compared with experiments in which annual or seasonal forcing are used. A similar unrealistic Gulf Stream separation is also obtained when the slope-water inflow at the northeast boundary is neglected. The experiments suggest that maintaining the density structure and the concomitant geostrophic flow in the northern recirculation gyre plays an important role in the separation of the Gulf Stream. The maintenance of the recirculation gyre is affected by heat transfer, wind stress, and slope-water inflow. The heat transfer involves several processes: lateral eddy transfer, surface heat flux, and vertical mixing. Further improvement of the Gulf Stream separation and climatology are obtained when seasonal changes in the lateral temperature and salinity boundary conditions are included.

The seasonal climatology of the model calculations compare reasonably well with the observed climatology. Although total transports on open boundaries are maintained at climatological values, there are, nevertheless, large seasonal and spatial variations of Gulf Stream transport between Cape Hatteras and 62°W. These changes are accompanied by transport changes in the northern recirculation gyre.

1. Introduction

Despite extensive observational and numerical studies in recent years, our understanding of the small- to mesoscale dynamics of western boundary currents and the Gulf Stream in particular is not complete. One reason is the difficulty of simulating all the processes affecting these jets. Bottom topography, nonlinear instabilities, mesoscale eddy activity, horizontal and vertical mixing, and air–sea interaction are a few of the processes that influence the Gulf Stream.

Eddy-resolving, quasigeostrophic models have been used to study the dynamics of eddies and meanders and their effect on the mean circulation in the vicinity of the Gulf Stream (e.g., Holland and Schmitz 1985; Robinson et al. 1988). These models are simple enough to allow high grid resolution so that mesoscale eddies are resolved. However, they lack some degree of realism; they neglect, for example, thermodynamics, internal and external gravity waves, and the direct effect of bottom topography and coastal dynamics. Spall and Robinson (1990) demonstrated some of the deficiencies of quasigeostrophic dynamics—for example, the restrictions of small Rossby number—by comparing a quasigeostrophic model of the Gulf Stream to a primitive equation model. Nevertheless, primitive equation models also fall short of providing realistic climatology and variability for the Gulf Stream area.

One of the major unsettled problems in numerical simulations of the Gulf Stream is the separation of the jet from the coast at Cape Hatteras; modeled Gulf Streams tend to separate from the coast farther north than does the observed stream. Thompson and Schmitz (1989), using a two-layer primitive equation regional model, demonstrate the sensitivity of the separation process to the bottom topography and to an imposed deep western boundary current (DWBC). They suggest that increasing the vertical resolution and allowing surfacing of temperature interfaces (which was not possible in their layered model) should improve the separation. Indeed, analytical models have shown that the ventilation of the thermocline plays an important role in the dynamics of western boundary currents (Luyten et al. 1983; Veronis 1981). Moreover, the

Corresponding author address: Dr. Tal Ezer, Princeton University, Program in Atmospheric & Oceanic Sciences, P.O. Box CN 710, Sayre Hall, Princeton, NJ 08544-0710.

ventilated thermocline may be strongly affected by surface heat flux transfer (Cushman-Roisin 1987). Therefore, it seems that primitive-equation numerical models should take into account more realistic air–sea interaction, including wind stress and heat flux exchange. The North Atlantic numerical model presented by Bryan and Holland (1989) has most of these ingredients, including 30 vertical levels and surface heat and salt fluxes. The latter model simulates the circulation in the North Atlantic reasonably well. However, in the Gulf Stream area the temperatures predicted by the model are significantly larger, by as much as 5°–10°C north of the Gulf Stream, than the observed temperatures, and the separation point is farther north than that observed.

Mellor and Ezer (1991) show that starting from observed temperature and salinity fields and without surface heat flux, their primitive equation model generated realistic climatology and separation for up to a year or more; later, the separation point moved north as in other models. As will be shown here, realistic separation of the Gulf Stream can be achieved if surface heat flux and wind stress are included in the same model. Therefore, we perform sensitivity studies to indicate the effect of different forcing on the separation of the Gulf Stream.

Although not all the processes affecting the separation of the Gulf Stream are understood, it seems that the dynamics of the slope water (Zheng et al. 1984) and the DWBC (Thompson and Schmitz 1989) have an important role. The effects of surface cooling on possible shifting in the Gulf Stream path have been demonstrated in analytical models (e.g., Nof 1983; Nurser and Williams 1990) and may be evident in the interannual shifting of the Gulf Stream as observed, for example, by Ionov et al. (1986) and Auer (1987). While it is obvious that wind stress and heat flux are important to the large-scale general circulation of oceanic gyres and jets, a question, however, exists as to whether or not local atmospheric forcing has any effect on simulations of the Gulf Stream in a regional model. Moreover, can regional models simulate the seasonal variations of the Gulf Stream? Such variations have been observed for the Gulf Stream sea surface height (Fu et al. 1987), transport (Worthington 1976), and even for the near-bottom flow under the Gulf Stream (Ezer and Weatherly 1991).

It is difficult to compare different models. For example, compared to the Bryan and Holland (1989) model, the model used here includes the coastal ocean, a second-order turbulence closure scheme, and a heat flux scheme that includes a feedback term. This model is also a regional model which, in contrast to a basin-scale model, is greatly affected by lateral boundary conditions.

In recent years, data assimilation (altimetry data in particular) in ocean models promises possible nowcast and forecast capability. However, data assimilation may depend on the model climatology (as with the data assimilation technique of Mellor and Ezer 1991), thus improving the realism of the model climatology is important. Moreover, if the model tends to depart from reality (as in the case of the Gulf Stream separation problem) its forecast capability is probably degraded. Thus, we study here the annual and seasonal climatologies of the model and compare them with observed climatologies in order to understand the dominant elements needed for realistic numerical simulations of the Gulf Stream.

In sections 2 and 3 we first briefly describe the model and the numerical experiments. Next, in section 4, we describe and discuss sensitivity studies to understand the effects of surface heat flux and wind stress forcing on Gulf Stream separation. In section 5, sensitivity studies of the effects of lateral boundary conditions are presented. In section 6, the simulated seasonal variations of the Gulf Stream are compared with observed climatologies, and finally, in section 7, we offer conclusions.

2. The ocean model

a. The model grid and initialization

The numerical ocean model that is used in this study is the one described in detail by Blumberg and Mellor (1987). It has been previously used in the South Atlantic Bight (Blumberg and Mellor 1983), Delaware Bay (Galperin and Mellor 1990a,b), the Hudson–Raritan estuary (Oey et al. 1985a,b), the Gulf of Mexico (Blumberg and Mellor 1985), and the Gulf Stream (Mellor and Ezer 1991), and is actively being applied in other regions of the World Ocean. The model domain and the boundary conditions in the current study are the same as in the study of Mellor and Ezer (1991) with three exceptions. First, the number of vertical layers is now 15 instead of 12 (the resolution in the upper mixed layer is increased such that the sigma levels are 0, −0.002, −0.004, −0.008, −0.016, −0.031, −0.063, −0.125, −0.25, −0.375, −0.5, −0.625, −0.75, −0.875, −1). Second, the vertical mixing coefficients are now provided by the turbulence closure scheme of Mellor and Yamada (1982) instead of fixed coefficients. Third, the surface boundary condition now includes heat flux exchange between the ocean and the atmosphere. The effect of these changes will be discussed in this paper.

The model has a bottom-following, vertical sigma coordinate system and a coastal-following, horizontal curvilinear orthogonal grid. Further aspects of the sigma coordinates are discussed by Mellor and Blumberg (1985). The horizontal resolution downstream of Cape Hatteras is about 20 km. The prognostic variables of the model are the free surface η, potential temperature T, salinity S, and velocity (u, v, w). The density, $\rho(T, S, p)$, is calculated from the potential temperature, salinity, and pressure, using an equation of state devised by Mellor (1991), which agrees with the UNESCO

formulas but is computationally simpler. Figure 1a shows the model grid and the lateral inflow/outflow discussed below. Figure 1b shows the bottom topography in the region. Further aspects of the numerical techniques and the dynamic equations can be found in the aforementioned papers.

b. The lateral boundary conditions

At the southern boundary of the model, at the Florida Straits, a constant inflow transport of 30 Sv (1 Sv $\equiv 10^6$ m^3 s^{-1}) is prescribed and is distributed according to measurements obtained during the Subtropical Atlantic Climate Studies (STACS; Leaman et al. 1987). At the northeastern boundary of the model, along the continental slope, a constant barotropic inflow transport of 40 Sv is prescribed. This flow is part of the northern recirculation gyre (Mellor et al. 1982; Richardson 1985; Hogg et al. 1986). An additional transport of 30 Sv is distributed along the model's southeastern boundary from 27°N to 32°N, wherein the vertically averaged inflow velocity is constant. This inflow is the continuation of the subtropical recirculation gyre south of the Gulf Stream (Worthington 1962; Mellor et al. 1982). The total of 100 Sv is allowed to exit the domain on the eastern boundary between 36° and 39°N. The locations of these inflow/outflows are indicated in Fig. 1a. Except for the Florida Straits and the northeastern slope flow, the rest of the open boundaries are governed by the Sommerfeld radiation condition. Therefore, although the total transport on the open boundaries is prescribed, the internal velocities are free to adjust geostrophically to the density field. Temperature and salinity on the open boundaries are locally upwinded. When flow is into the model domain, they are prescribed from the observed climatologies, and boundary information is advected into the model domain.

c. The surface boundary conditions

The surface boundary conditions are zero salinity flux, but nonzero heat flux and wind stress. We describe here only the surface boundary conditions for heat flux and wind stress; the bottom-flux boundary conditions are adiabatic; the stress condition can be found in the papers cited in section 2a. The surface heat flux is obtained from the 2° × 2° monthly averaged climatologies of the Comprehensive Ocean–Atmosphere Data Set (COADS) analyzed by Oberhuber (1988), together with a one-way model feedback scheme. We discuss next the case of monthly forcing. The net downward heat flux at the surface of the model, $Q(x, y, t)$, is calculated by

$$Q = Q_{\text{obs}} + \left(\frac{\partial Q}{\partial T}\right)_{\text{obs}} (T - T_{\text{obs}}) \qquad (1)$$

where Q_{obs} is the observed climatological, net downward heat flux excluding the shortwave radiation, Q_s. The second term in (1) is a feedback term such that

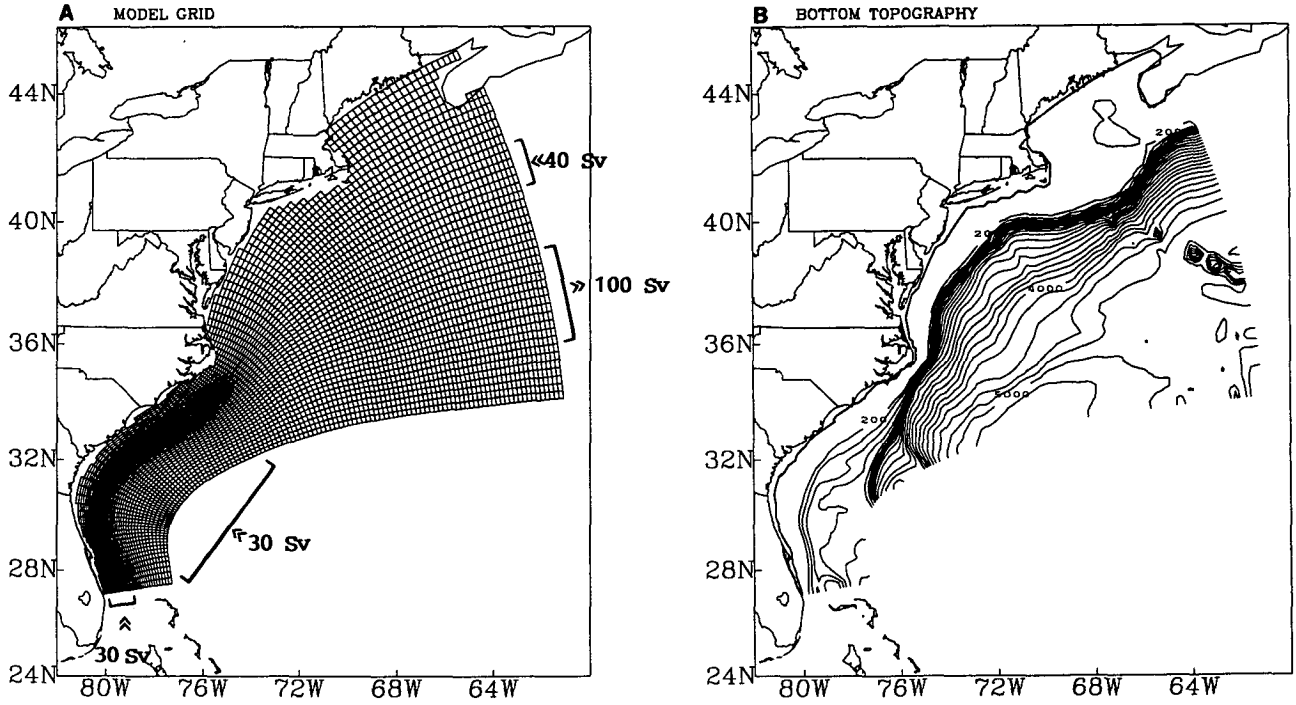

FIG. 1. (a) The curvilinear orthogonal model grid. Prescribed inflow/outflow transport boundary conditions are indicated. (b) The bottom topography of the model; the contour interval is 200 m; the thick contour is the land boundary of the model at 20-m depth.

additional local cooling or heating is applied where model surface temperature, T, is greater or less than the observed climatology, T_{obs}. This allows, for example, cooling of warm core eddies. The observed net heat flux $Q_{obs} + Q_s$ and the observed surface temperature T_{obs} (interpolated into the model grid) for January, July, and their annual averages are shown in Fig. 2. All the observed fields, including $(\partial Q/\partial T)_{obs}$ and Q_s, are obtained from the COADS and can be found in Oberhuber's atlas. An approximate average value for $(\partial Q/\partial T)_{obs}$ is -50 W m^{-2} K^{-1}. The use of Eq. (1) is equivalent to a calculation of heat flux wherein air temperature, humidity, and cloud cover are fixed climatologically but the SST is derived from the model. Note that along the Gulf Stream path, there is maximum cooling in the winter (e.g., in January) and relatively less warming in the summer (e.g., in July).

At the model surface,

$$Q = K_H \frac{\partial T}{\partial z}, \quad z \to \eta(x, y, t) \tag{2}$$

where K_H is the vertical diffusivity. The shortwave radiation Q_s in the model is absorbed in the upper several meters and is added directly to the heat equation,

$$\frac{\partial T}{\partial t} = (\text{advective and diffusive terms}) + \frac{\partial R}{\partial z} \tag{3a}$$

$$R = Q_s \exp(\lambda z) \tag{3b}$$

where the coefficient, λ, is chosen to fit the tabulated attenuation function of Jerlov (1976). In this study, surface salinity fluxes are neglected. However, more recent experiments in which surface salinity fluxes and river runoff are added show a small effect on the Gulf Stream climatology.

The surface wind stress is calculated from the monthly climatologies of winds obtained from the COADS (Wright 1988). The magnitude of the wind stress at a given time and position is $|\tau| = \rho_0 C_D V^2$ where V is the synoptic wind speed. To estimate the synoptic wind from the climatological wind velocity data [which is averaged in time (monthly) and space ($2° \times 2°$)], we approximate the synoptic wind by $V = \bar{V} + V'$, where V' is the perturbation about the mean $\bar{V}$, and neglect cross correlation between the mean and the perturbation. Therefore, the wind stress components are taken as

$$\tau_x = A\rho_0 C_D \bar{V}^2 \frac{\bar{u}}{(\bar{u}^2 + \bar{v}^2)^{1/2}} \tag{4a}$$

$$\tau_y = A\rho_0 C_D \bar{V}^2 \frac{\bar{v}}{(\bar{u}^2 + \bar{v}^2)^{1/2}} \tag{4b}$$

where $\bar{V}$, $\bar{u}$, $\bar{v}$ are the climatological averages of the wind speed and velocity components and $A = 1 + \sigma^2/\bar{V}^2$; the ratio between the variance and the average wind speed squared is taken as 0.25 (Wright 1988). The drag coefficient C_D is calculated from the observed wind speed according to Garratt (1977) and includes a stability factor that depends on the difference between the observed air temperature and the model surface temperature according to Kondo (1975). Therefore, there is a one-way feedback effect in the transfer of momentum from the atmosphere to the ocean such that the wind stress increases over areas of relatively warmer water. The resulting wind stress over the model domain is comparable to previous studies (e.g., Hellerman and Rosenstein 1983; Trenberth et al. 1990) and is shown in Fig. 3 (using the observed air and sea temperatures to calculate the drag coefficient). Note the maximum wind stress and convergence along the Gulf Stream path, which may be the result of strong convection in the atmospheric boundary layer. The boundary condition at the surface is

$$\frac{1}{\rho_0}(\tau_x, \tau_y) = K_M \frac{\partial}{\partial z}(u, v), \quad z \to \eta(x, y, t) \tag{5}$$

where ρ_0 and K_M are the water density at the surface and the vertical kinematic viscosity, respectively. Here, u and v are the model velocity components near the surface and should not to be confused with the wind components in Eq. (4). The monthly climatological wind speed and wind components are linearly interpolated into each model time step.

3. The numerical experiments

The model is initialized with climatological temperatures and salinities analyzed by Kantha et al. (1986) on 30 vertical levels and a 1/4° × 1/4° grid and then interpolated to the model grid. The initial fields are shown in Mellor and Ezer (1991). The model then runs for 10 days diagnostically (T and S held constant) and then prognostically (with constant wind stress and heat flux) for 30 days. During the latter period, the Gulf Stream narrows and meanders, and eddies start to form. All the experiments described in this paper were initialized with the fields obtained after these 40 days. In the case of monthly forcing, this initial day corresponds to Julian day 90 (1 April), where 30 days in a month and 360 days in a year are stipulated.

In section 4, the inflow/outflow boundary conditions are held fixed while only surface boundary conditions vary in the experiments. Therefore, we study the response of the numerical model to local atmospheric forcing. Changes in the large-scale circulation of the subtropical gyre or seasonal variations in the flow at the Florida Straits are neglected here and will be discussed in section 5. All of these runs start from the same initial conditions, and include five years of simulation. We define the model climatology of each run as the average over five years. Ten-year experiments (not reported here) indicate that the 5-year climatology is not significantly different from the 10-year climatology.

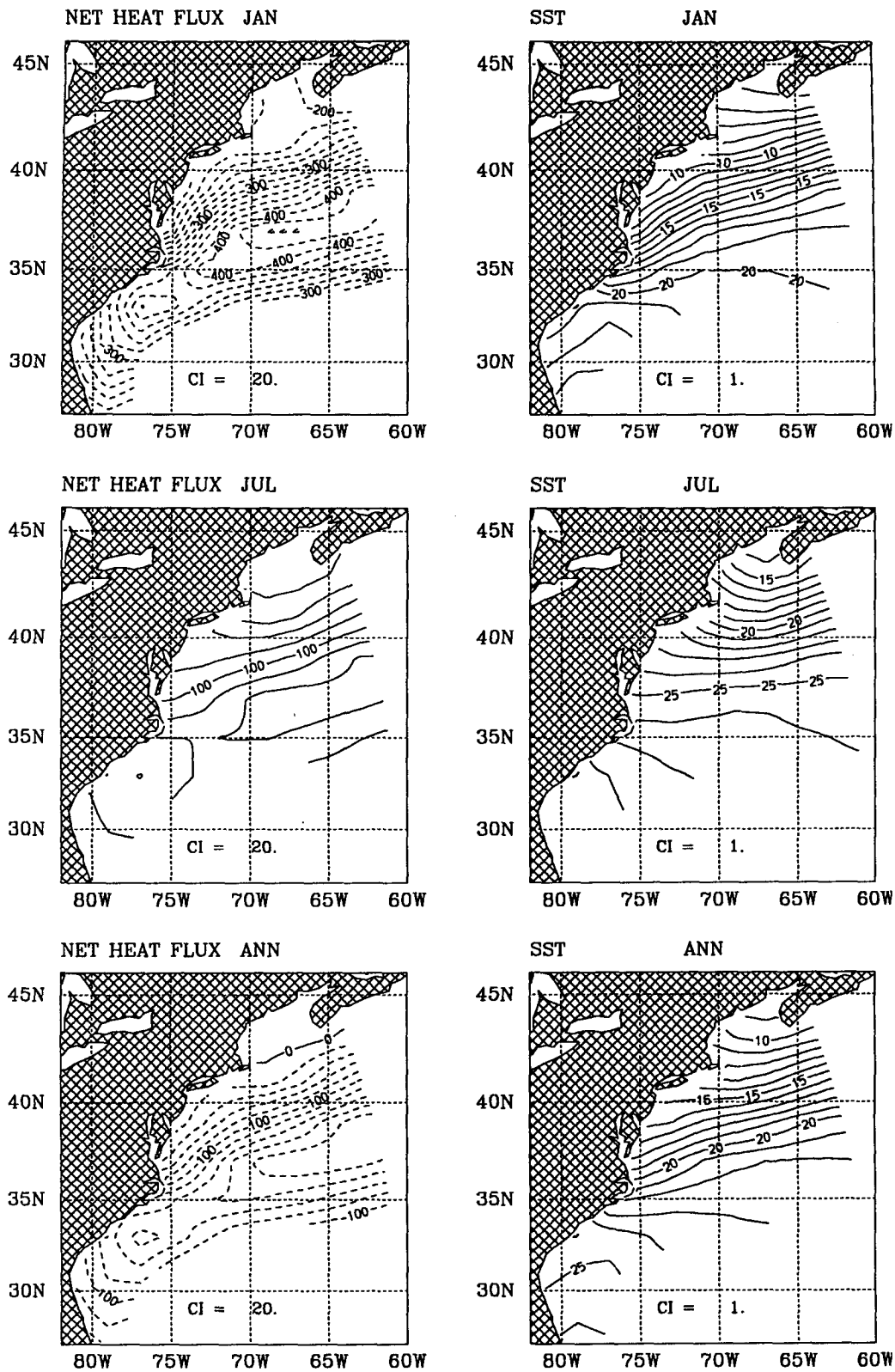

FIG. 2. The net downward heat flux (left panel) and the surface sea temperature (right panel) for January (upper panel), July (middle panel), and annual average (lower panel), obtained from the COADS and interpolated to the model grid. The contour intervals are 20 W m^{-2} and 1°C for the heat flux and the temperature, respectively.

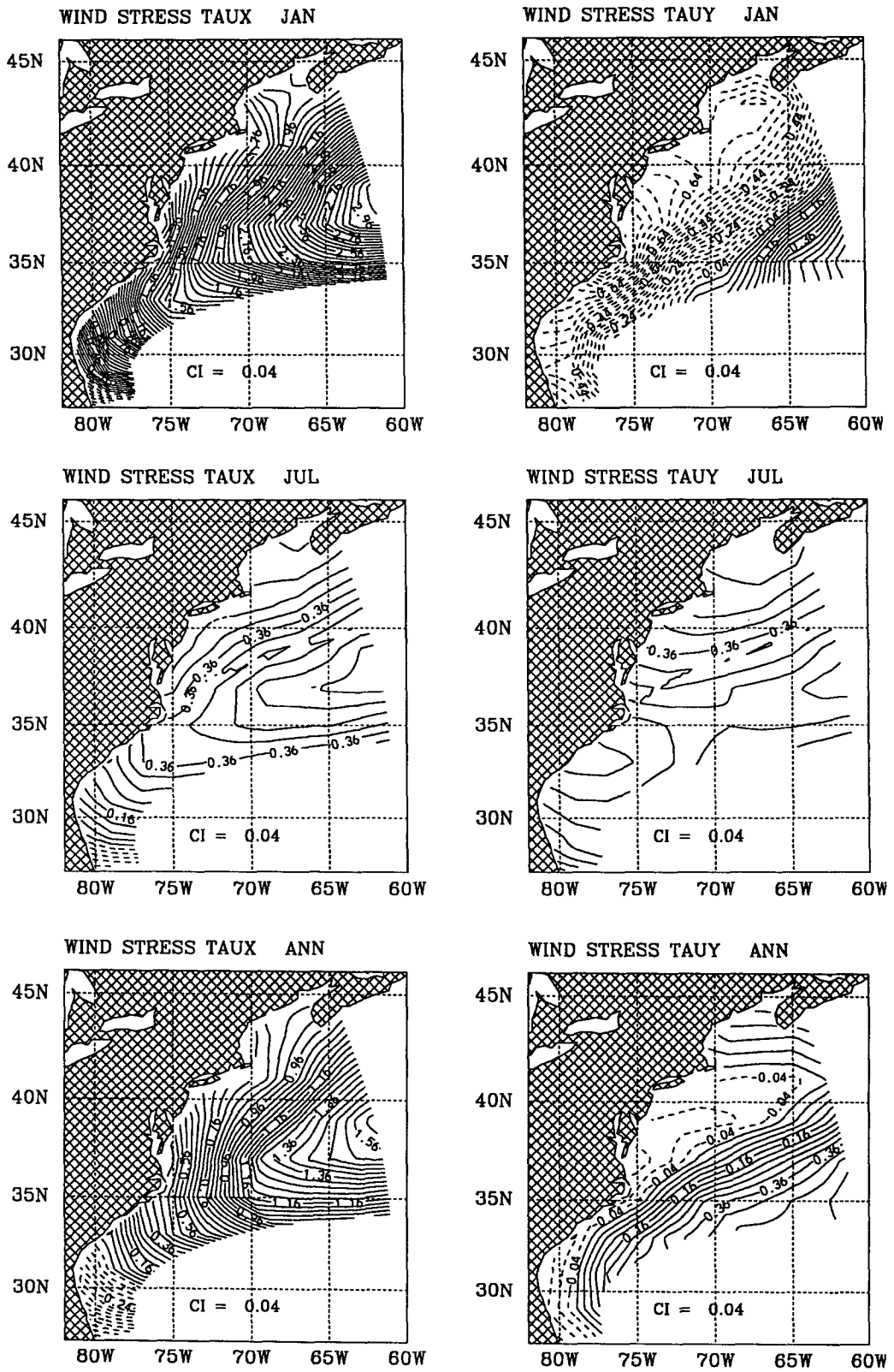

FIG. 3. The eastward wind stress component, τ_x, (left panel) and northward component, τ_y, (right panel) for January (upper panel), July (middle panel), and annual average (lower panel), calculated from the COADS winds and interpolated into the model grid. The contour intervals are 0.04 dyn cm^{-2}.

In Fig. 4, the rms elevation is obtained from the Geosat altimetry data and will be compared with the model data later. The altimetry data of the areas deeper than 1000 m were interpolated into the model grid, using the optimal interpolation scheme described by Mellor and Ezer (1991). Because of the smoothing nature of the optimal interpolation, Mellor and Ezer (1991) show that the rms elevation obtained by interpolating data sampled along Geosat tracks is only about 70% of the rms elevation obtained from data sampled at all model grid points. This, together with the fact that analysis of the raw data also involves smoothing, produces rms elevations that are smaller than reality. The general shape should be retained, however, and consists of maximum variability along the Gulf Stream path, with three maxima at 72°, 67.5°W, and at the eastern boundary. The latter coincides with the maximum in eddy kinetic energy west of the New England Seamounts as indicated by Richardson (1983). The two maxima south of the stream at ~35°N could be the result of cold-core eddy activity. As was shown by Mellor and Ezer (1991), there is significant similarity between the rms of surface elevation in the model and the eddy kinetic energy of the upper layers. Therefore, although we will restrict discussion to variability in surface elevation, similar results apply also to the surface eddy kinetic energy.

The experiments discussed in this paper are summarized in Table 1. Each simulation (with different surface or lateral boundary conditions) is for 5 years.

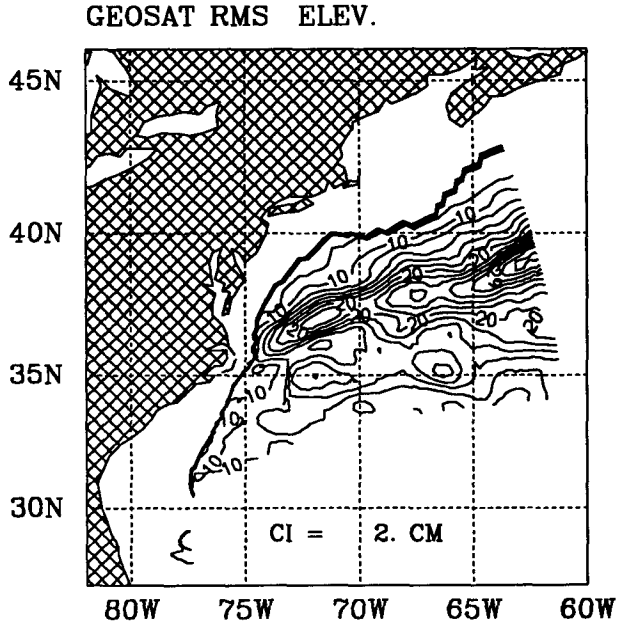

FIG. 4. The rms surface elevation obtained from Geosat altimetry data, collected between November 1986 and November 1988, and interpolated into the model grid. The thick line shows the 1000-m isobath; only data where the ocean depth is greater than 1000 m are used. The contour interval is 2 cm.

TABLE 1. The numerical experiments.

Experiment (Fig.)	Surface heat flux	Surface wind stress	Lateral *T, S*	Lateral *U, V*
1 (5a)	zero	annual	annual	annual
2 (5b)	annual	zero	annual	annual
3 (7a)	annual	annual	annual	annual
4 (7b)	monthly	monthly	annual	annual
5 (12a)	monthly	monthly	annual	no slope
6 (12b)	monthly	monthly	seasonal	annual

4. The effects of surface heat flux and wind stress

In the first three experiments, we study the effects of neglecting either surface heat flux or wind stress. The lateral boundary conditions are fixed now at the annual values as described in section 2b. In experiment 1 the model is forced at the surface by annual wind stress while surface heat flux is set to zero. In experiment 2, the annual atmospheric heat flux (including the feedback effect) is used at the surface boundary of the model while wind stress is set to zero. Both wind stress and surface heat flux are included in experiment 3. The total streamfunction and the mean and rms surface elevation for these three experiments are shown in Fig. 5a, Fig. 5b, and Fig. 7a, respectively. In experiments 1 and 2, a large anticyclonic meander dominates the circulation north and east of Cape Hatteras. This area is also associated with a large maximum rms elevation of about 40 cm. To understand the mechanism responsible for the peculiarity of the circulation with no heat flux or no wind stress, we examine some synoptic realizations. Figure 6 shows the surface elevation for the period 1 September to 16 November of the third year of experiment 1. On 1 September, a warm-core eddy is seen at 38°N, 72°W. Two weeks later, the eddy starts to decay, but on 1 October it interacts with the Gulf Stream and then separates again into a larger eddy on 16 October. It interacts with the Gulf Stream again to form a meander on 16 November. Similar events occur several times during the 5-year period. Warm-core eddies drift westward and become trapped in the western corner of the recirculation gyre. Since these eddies are warmer than the interior, they are subject to intense cooling.

We now call attention to the fact that, in all of our simulations, fairly realistic separation of the Gulf Stream at Cape Hatteras prevails for the first year. Then, in the beginning of the second year, the previously cold and denser recirculation gyre north of the stream warms and breaks down in the case of experiments 1 and 2. The gyre is warmed by eddy transfer of heat which, as we interpret the simulations, is inhibited by local wind-stress dynamics–Ekman southward transport near the surface and classical wind-stress curl reinforcement of the deeper gyre water (experiments 1 and 3) and by direct cooling of the gyre (experiments 2 and 3). The wind mixing may also par-

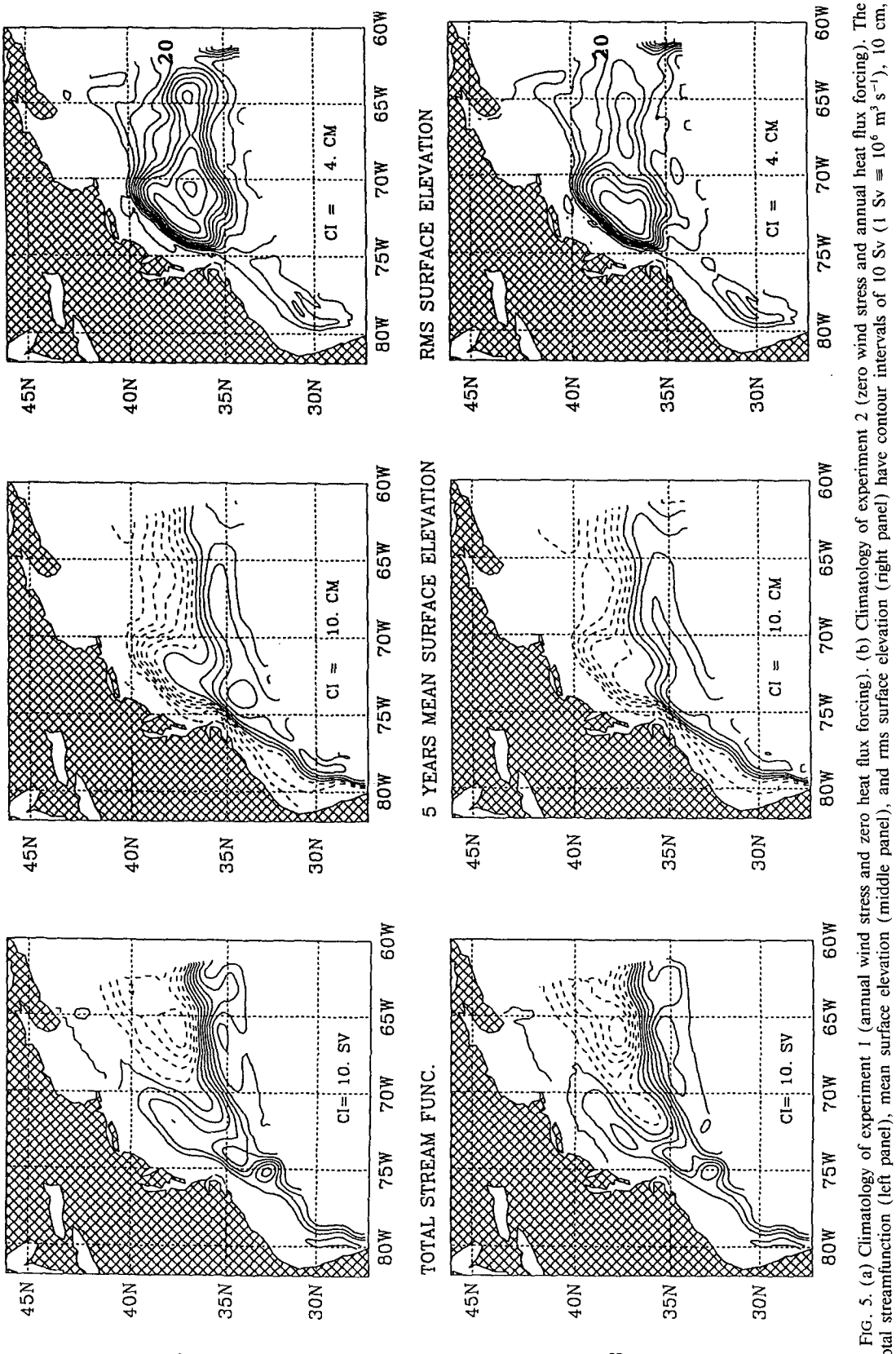

FIG. 5. (a) Climatology of experiment 1 (annual wind stress and zero heat flux forcing). (b) Climatology of experiment 2 (zero wind stress and annual heat flux forcing). The total streamfunction (left panel), mean surface elevation (middle panel), and rms surface elevation (right panel) have contour intervals of 10 Sv (1 Sv $\equiv 10^6$ m^3 s^{-1}), 10 cm, and 4 cm, respectively.

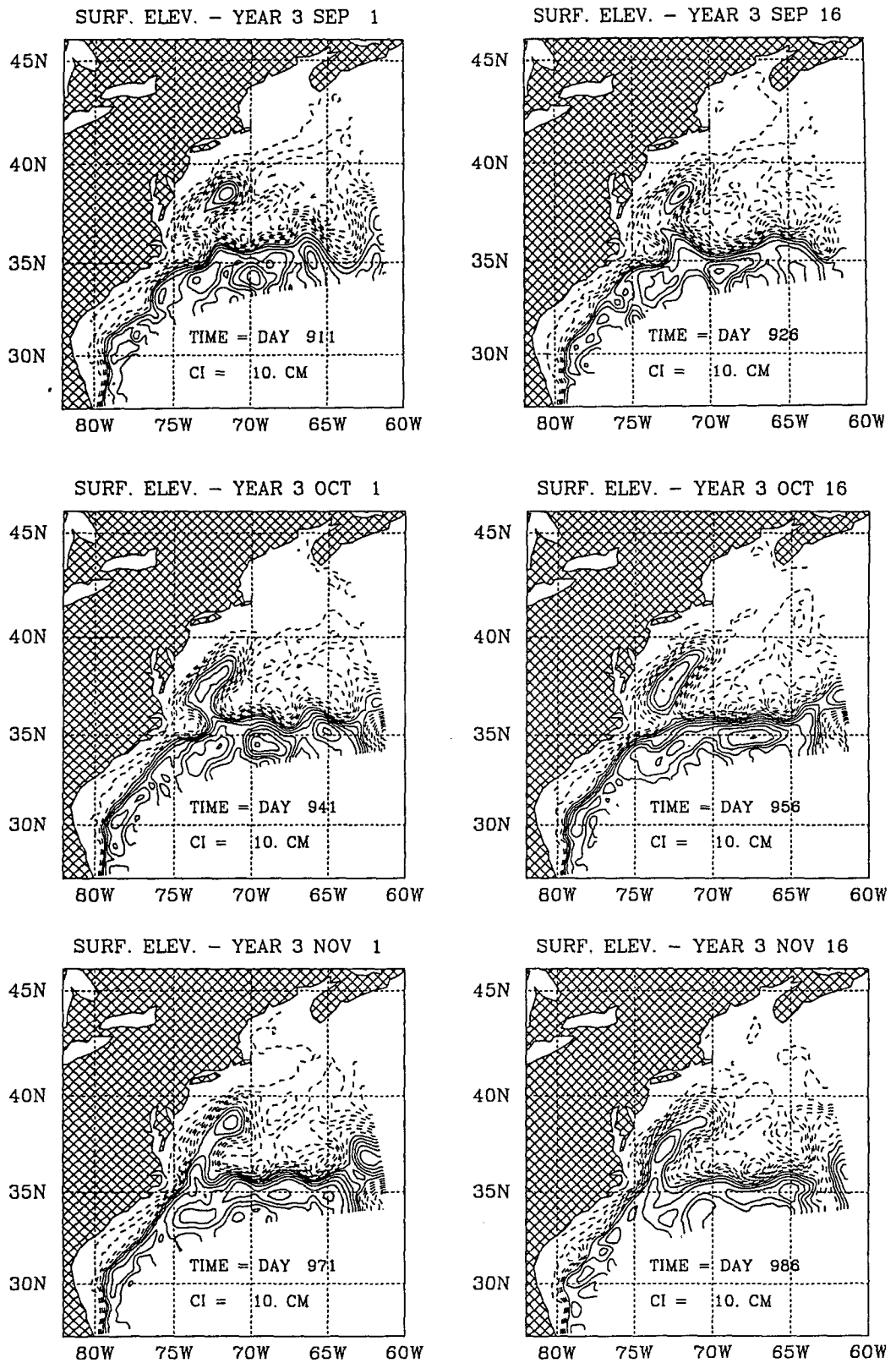

FIG. 6. Synoptic realizations of surface elevation in the third year of experiment 1, from 1 September to 16 November.

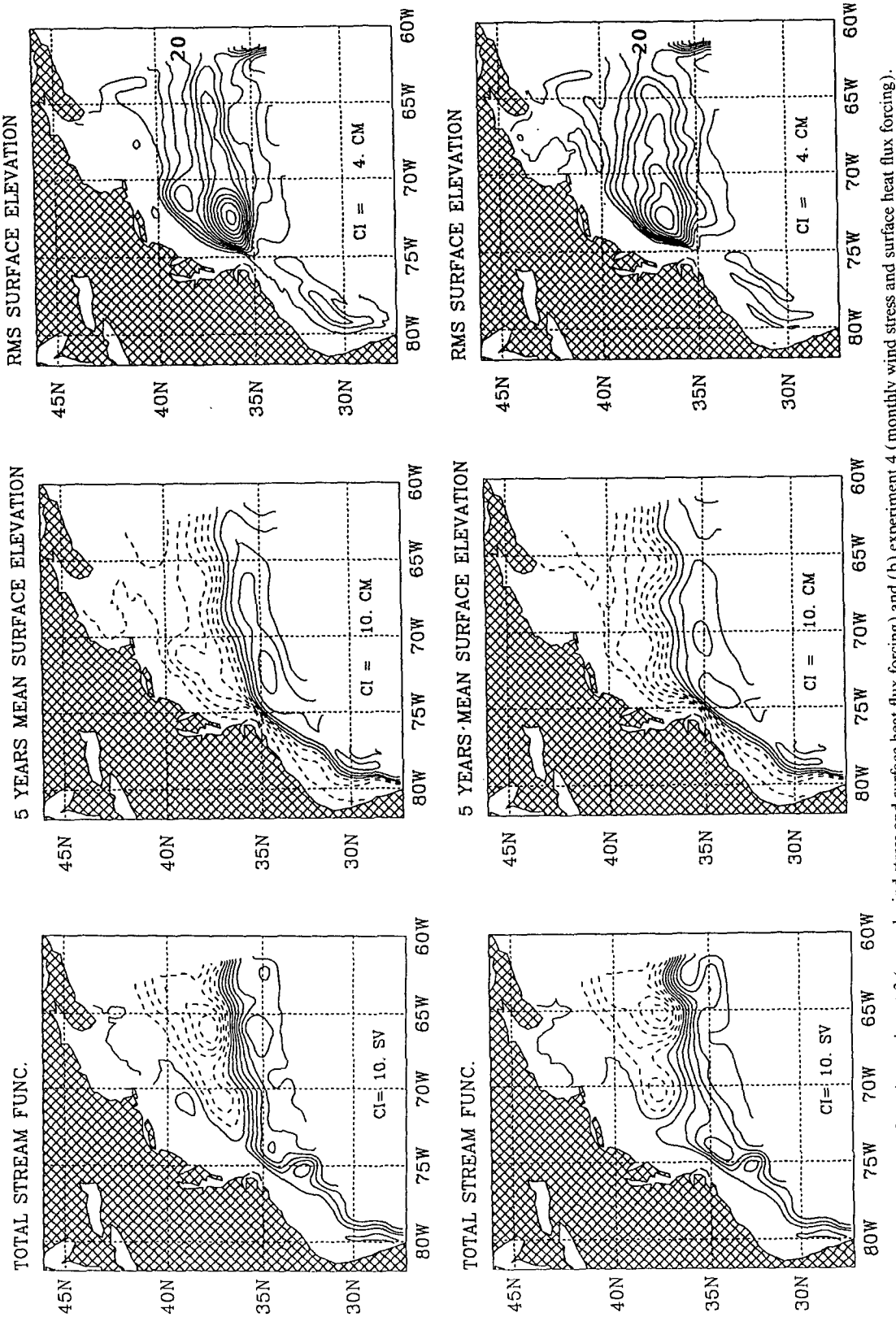

FIG. 7. As in Fig. 5 but for (a) experiment 3 (annual wind stress and surface heat flux forcing) and (b) experiment 4 (monthly wind stress and surface heat flux forcing).

ticipate in the penetration of surface cooling into the water column. Experiment 3, forced by surface wind stress and heat flux, resembles the observed Gulf Stream structure.

Comparing the variability of the surface elevation in experiments 1 and 2 (Fig. 5) to the observed variability (Fig. 4), we note the following differences. Near the open eastern boundary the variability of the surface elevation in the model is smaller than that observed. The boundary conditions suppress variability; eddies that might form east of 60°W and propagate westward are, of course, not represented in this regional model. Along the Florida shelf there is a maximum in the model variability, the result of the interaction of the stream with the topographic feature known as the "Charleston Bump." The Geosat data does not include this shallow area. However, the increase in variability, as well as the deflection of the modeled Gulf Stream by the bump, agrees with observations (e.g., Bane 1983; Olson et al. 1983). Downstream of Cape Hatteras there are three maxima of high variability in experiment 1 of the model simulation. Proceeding from west to east, the first high is the result of the unrealistic meander off Cape Hatteras. The second and the third maxima, at 71°W and at 64°W, are offset eastward by a few degrees, compared with the location of similar maxima in the observed variability. The maximum rms of surface elevation in the model is ~40 cm, while the observed maximum is 20–30 cm. Note that the rms obtained from the altimeter data is smaller than the true rms, as discussed in section 3. Although the mean Gulf Stream separation of experiment 3 is much more realistic compared to experiments 1 and 2, the variability off Cape Hatteras is still somewhat too large. This is the result of the fact that there are still periods of large meanders developing off the separation point, though not as frequently as in the previous experiments. Satellite-derived surface temperature data indicate that such meander events north of Cape Hatteras do occur from time to time, but on average, such events seem to be more frequent in the model than in the ocean. However, we are now able to report that experiments (not shown) duplicative of experiment 3 but with 20 vertical levels instead of 15 further improve the separation and variability patterns.

We now discuss some of the effects of the monthly forcing in experiment 4. The forcing has little effect on the mean flow between the Florida Straits and Cape Hatteras, where the bottom topography seems to control the Gulf Stream path. Downstream of Cape Hatteras, the Gulf Stream is on average wider and has larger permanent meanders in the monthly forced case (Fig. 7b) compared with the annually forced case (Fig. 7a). The variable wind and heat flux increase the variability of the stream by generating a seasonal shift in the Gulf Stream path. This can be seen in the rms elevation, where the area of large variability is wider in experiment 4. Note also the fact that the locations of the maxima in rms elevation are similar to their location in the observed rms elevation.

Since the heat flux seems to play an important role in the structure of the Gulf Stream, we now discuss it in more detail. The surface heat flux in the model includes the two terms in Eq. (1); one is due to the observed heat flux and the other is the feedback term that depends on the difference between the observed SST and the model SST. Figure 8 shows the 5-year average net heat flux of the model in experiment 3. The model heat flux, although larger by a factor of ≤ 2 than the observed heat flux without the feedback (i.e., Fig. 2), may not be unrealistic. It is quite possible that the COADS climatological heat flux underestimates the instantaneous heat flux in this area. For example, observations indicate very large cooling (more than 1000 W m^{-2}) during short periods of time when a cold air outbreak from the continent passes over the Gulf Stream during winter (Grossman and Betts 1990). Such events may not be represented in the smooth 2° × 2° monthly averages. Another test of the model surface forcing will be a comparison (shown later) with satellite-derived SST; we will see if the surface forcing produces some of the features that are clearly missing in the smoothed COADS SST shown in Fig. 2 and used in the heat flux feedback term.

Another aspect of the surface forcing is its possible effect on the deep circulation. There is observational evidence that seasonal variations of the Gulf Stream may be detected even in the abyssal near-bottom flow (Ezer and Weatherly 1991). Moreover, the seasonal changes in the upper mixed layer affect the ventilation

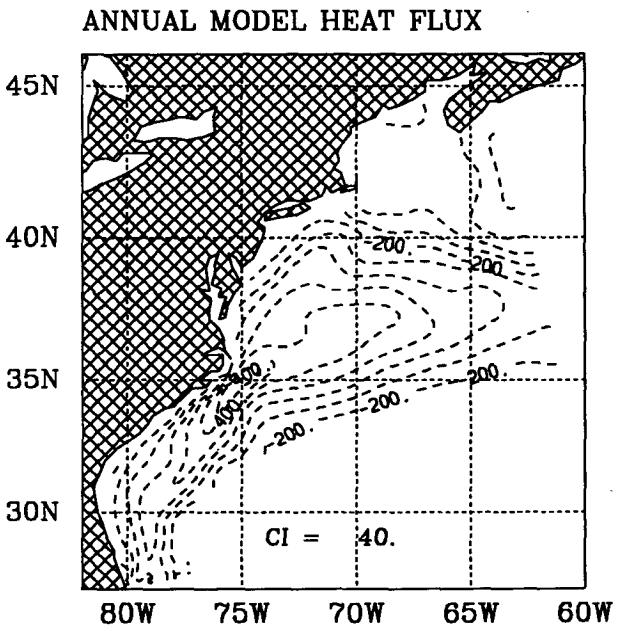

FIG. 8. The 5-year averaged net surface heat flux of the model (experiment 3). The contour interval is 40 W m^{-2}.

of the thermocline, which plays an important role in the dynamics of western boundary currents (Luyten et al. 1983; Veronis 1981; Cushman-Roisin 1987). For example, it is important to know the period of time in which winter cooling and upper-ocean mixing are sufficient to allow possible subduction. Therefore, we examine the penetration of the surface forcing into deeper layers. Figure 9 shows the area-averaged temperature at four depths for experiments 1 to 4. The averages are over the model area where the bottom depth is greater than 1000 m, that is, the extension of the Gulf Stream and the recirculation gyre, excluding the continental shelf and slope. In the deep layers (say below 500 m) the variations seem barotropic and related probably to the meandering of the Gulf Stream. The upper 100 m is highly stratified in the case of zero heat flux (Fig. 9a) with surface temperature higher by about 2°C than the cases of annual heat flux. There is slightly less mixing in the case of zero wind stress (Fig. 9b) than the case of annual wind stress (Fig. 9c). Monthly heat flux

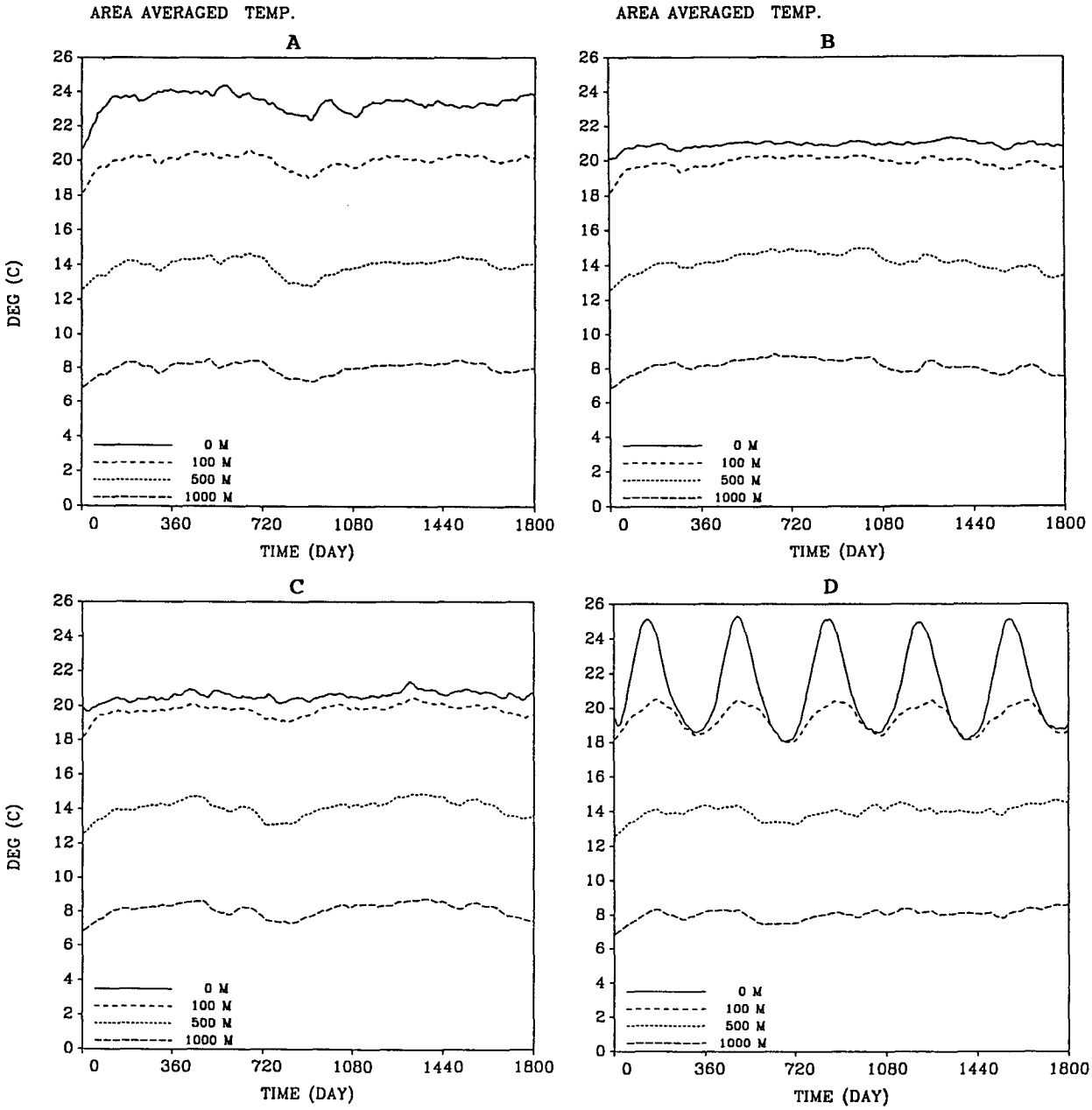

FIG. 9. Area-averaged temperature at four depths (excluding regions shallower than 1000 m) as a function of time for (a) experiment 1, (b) experiment 2, (c) experiment 3, and (d) experiment 4. Day 0 starts on 1 April.

results in the most stratified ocean during the summer and a deep mixed layer during the winter (Fig. 9d). The amplitude of the seasonal variations is about 6°C at the surface and about 2°–3°C at 100 m. Note that since this region has, on average, negative net surface heat flux (Fig. 2), it implies a positive heat flux through the lateral boundaries (mostly by advection of warm water from the Florida Straits and the subtropical gyre). Thus, if surface heat flux is neglected, warming of the domain as in Fig. 9a is expected.

The area-averaged velocities are less affected by the surface conditions than are temperatures (Fig. 10). The largest surface velocities are found in the run with no heat flux and annual winds (Fig. 10a) and not in the run with the stronger monthly winds (Fig. 10d). This is the result of the fact that, in experiment 1, the winds drive a much shallower upper mixed layer, and there is less loss of energy by mixing because of the stably stratified upper layer. Unlike the simulated temperature field (Fig. 9d), no apparent annual pattern in the velocity field is seen in the simulation with the monthly forcing (Fig. 10d); the flow variability is dominated by

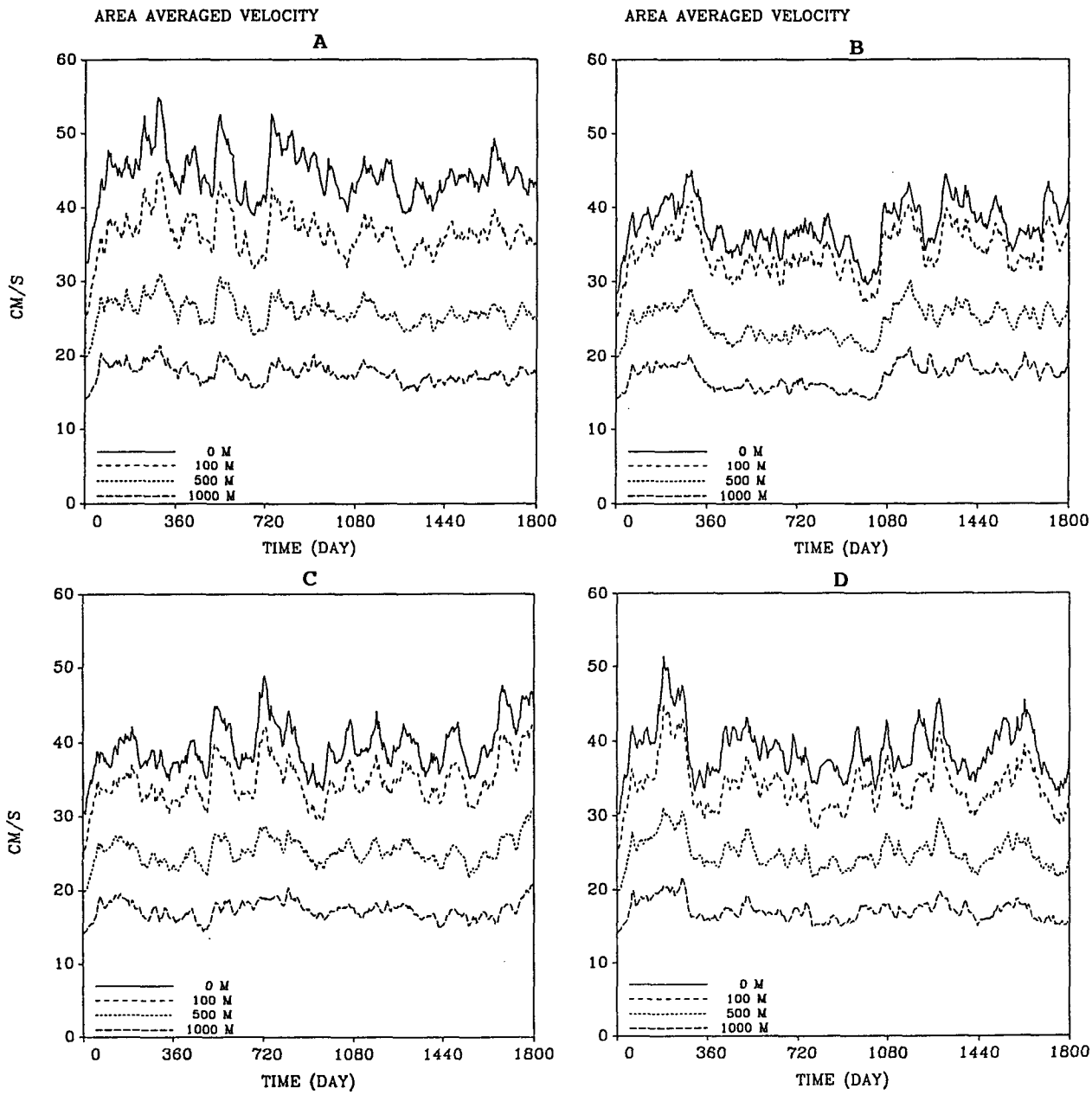

FIG. 10. As in Fig. 9 but for the area-averaged velocity.

the meandering Gulf Stream with coherent structures penetrating to at least 1000 m.

A more detailed look at the mixed layer for experiments 3 and 4 is shown in Fig. 11. The stratification of the upper layer shows an ~80-m thick mixed layer in the annual forcing case and ~150-m thick mixed layer during the winter in the monthly forcing case. During the summer, the stably stratified seasonal thermocline extends from the surface to a depth of about 100 m. Note that the maximum surface temperature is obtained in August and September, while the maximum temperature at 100 m is obtained about two months later. Below the mixed layer, vertical mixing and downward advection along density surfaces transport the surface winter water to deeper layers. We note also that the fluctuations of the temperature decay downward in the monthly forcing case, but decay upward in the annual forcing case. Probably, the source of the deep fluctuations are fluctuations in velocities on the lateral boundaries.

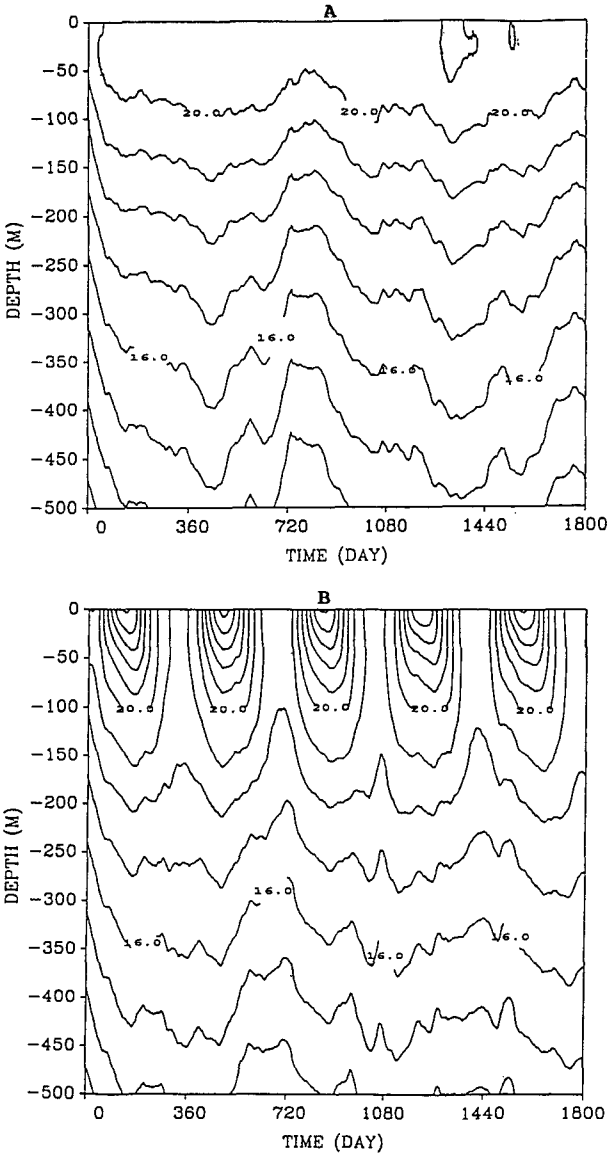

FIG. 11. The temperature structure in the upper 500 m, in experiment 3 (upper panel) and experiment 4 (lower panel). Contour interval is 1°C.

5. The effects of lateral forcing

a. The effect of slope-water inflow

The current regional model does not contain the entire northern recirculation gyre, which extends farther east of the model domain (Hogg et al. 1986). Therefore, the circulation north of the Gulf Stream depends on the imposed boundary conditions as demonstrated by Thompson and Schmitz (1989). In their study, imposing large outflow (representing the DWBC) on the south boundary of the lower layer results in southward shift of the Gulf Stream path though, even with 40 Sv of the DWBC, the Gulf Stream still tends to overshoot and shows a large unrealistic meander downstream of Cape Hatteras. We follow their study; however, in our case, the DWBC is not imposed as outflow, but is generated by the model as a continuation of the slope-water inflow at the northeastern boundary as shown by Mellor and Ezer (1991).

In experiment 5, the model was forced at the surface by monthly heat flux and wind stress, but the 40 Sv of slope-water inflow at the northeastern boundary (Fig. 1a) is shut off. Thus, only 60 Sv exit the model on the eastern boundary. The total streamfunction (calculated from the vertically averaged horizontal velocity) and the surface elevation (both averaged over five years) show a wide meander downstream of Cape Hatteras; only a limited recirculation gyre is seen north of the Gulf Stream (Fig. 12a). The rms surface elevation in this experiment has a dominant but unrealistic maximum at 72°W (compared with Fig. 4) that is associated with the location of the large meander downstream of Cape Hatteras. We note that the DWBC is developed by the model even without the imposed inflow (not shown), although it is weaker than the cases of imposed slope-water flow. Although the separation looks qualitatively similar to the results of Thompson and Schmitz (1989), there are some differences. Their study shows that the addition of 40-Sv DWBC shifts the entire Gulf Stream at least 2° south and changes considerably the eddy kinetic energy, while when we compare experiment 5 to the case where slope-water inflow is reinstated, we observe more of a local effect, the generation of a meander near the separation point. The important role of the cold slope-water inflow in the dynamics of the Gulf Stream is evident in observations, as shown by Zheng et al. (1984). In our experiments, neglecting the slope-water inflow results in a warming of the northern recirculation gyre and a weakening of the DWBC; both affect the separation of the Gulf Stream.

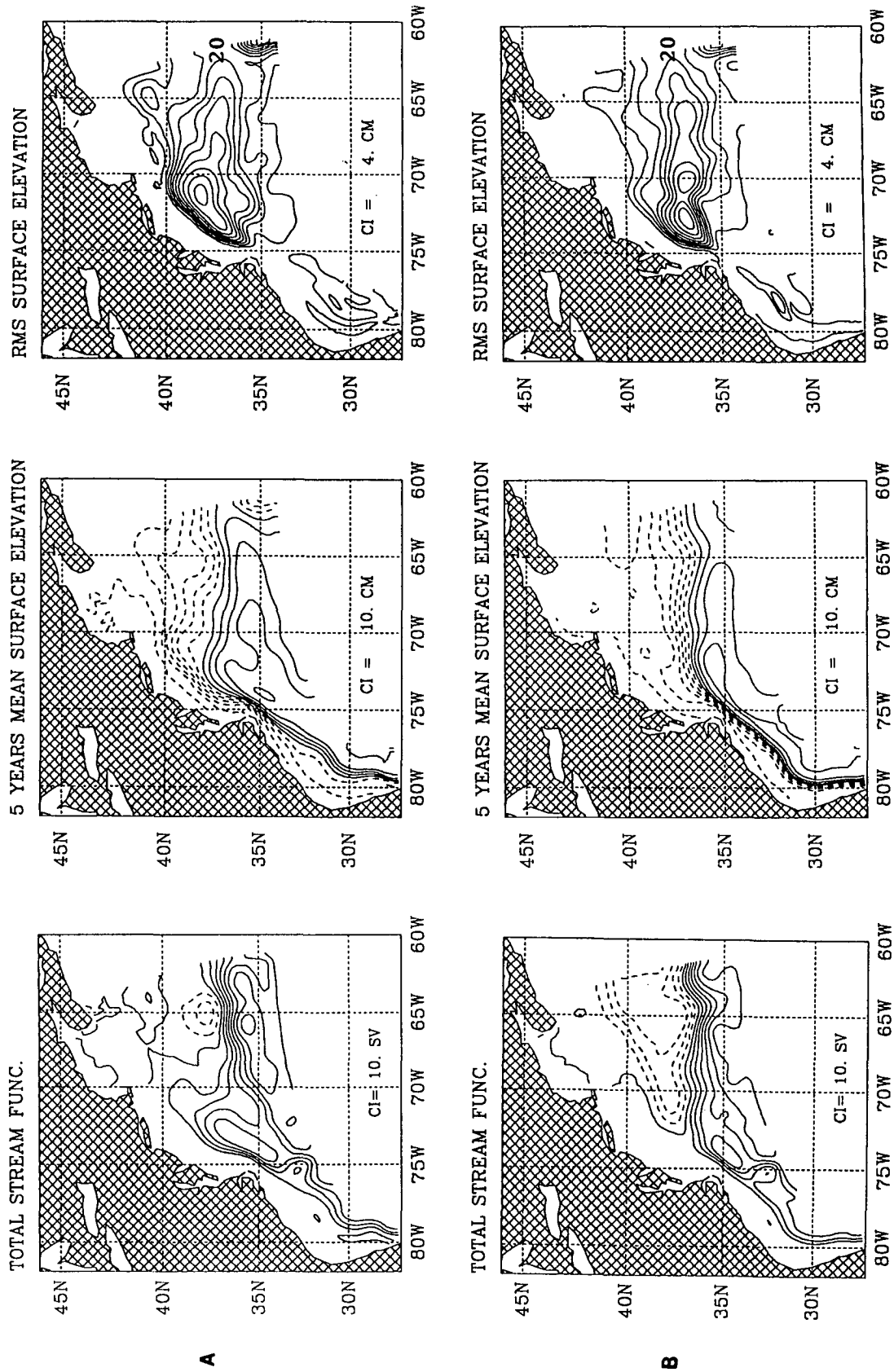

FIG. 12. As in Fig. 5 but for (a) experiment 5 (monthly wind stress and surface heat flux forcing, but zero slope-water inflow) and (b) experiment 6 (monthly wind stress and surface heat flux forcing, but seasonal thermal boundary conditions).

We conclude that the recirculation gyre and maintenance of its thermodynamic structure is necessary to Gulf Stream separation at Cape Hatteras.

b. The effect of seasonal lateral boundary conditions

In all of the experiments discussed thus far, the temperature and the salinity on the open boundaries were held fixed at the annual observed climatological values. In experiment 4, seasonal variations were obtained only through the surface heat flux and wind stress. However, seasonal variations at the lateral boundaries may play an important role in the dynamics of the Gulf Stream, especially at the Florida Straits (Niiler and Richardson 1973; Schott et al. 1988) and at the northeastern boundary where the slope water is found (Zheng et al. 1984). Therefore, we now add experiment 6 in which seasonal variations of temperature and salinity are included on the boundaries. We use the climatology of four seasons (Kantha et al. 1986), defined as follows: Winter is January to March; spring is April to June; summer is July to September; fall is October to December. The temperature and salinity on the boundaries are now time dependent, linearly interpolated between seasons. The surface forcing is monthly as in experiment 4.

The 5-year climatology of the total streamfunction, the surface elevation, and the rms surface elevation of experiment 6 are shown in Fig. 12b, and should be compared with experiment 4 (Fig. 7b). With seasonal thermal boundary conditions, the Gulf Stream separation is improved, and the meander downstream of Cape Hatteras almost disappears. The Gulf Stream is more robust, having a larger elevation gradient across the stream, and the variability seems more realistic as well. The effects of the seasonal boundary conditions are especially important in the southern portion of the domain, along the Florida shelf. We should keep in mind that the seasonal variations at the Florida Straits are imposed on the temperature and the salinity and not on the velocities; thus, changes are due to the nearly geostrophic adjustment of the flow field to the baroclinic structure. The Gulf Stream shifts shoreward, is closer to the continental slope, and is in closer agreement with observations. The area of large variability in the southern portion of the model is now concentrated downstream of the Charleston Bump, an indication of the disturbances induced by this topographic feature.

6. The seasonal variations of the Gulf Stream

We now examine the monthly surface forcing and seasonal lateral forcing calculations and compare the seasonal climatology of experiment 6 with observations. The satellite Multi-channel Sea Surface Temperature (MCSST), obtained from the National Oceanographic Data Center and analyzed by the Institute for Naval Oceanography, is used. It includes two years of data, archived twice a week from January 1987 to December 1988, interpolated from the $1/8° \times 1/8°$ grid to the model grid. These data are independent of the COADS used in the feedback of the heat flux calculations. They have much better resolution and more realistically represent the Gulf Stream region.

The seasonal climatology is defined as the average over all the records included in each of the four seasons. Only data north of 30°N is used. The seasonal observed surface temperatures are shown in Fig. 13, and the seasonal model surface temperatures are shown in Fig. 14. Generally, the agreement is quite good, but some differences are apparent. For example, the maximum temperature gradient in the model is found farther north in the west and farther south in the east, compared with the observed SST. Along the Florida shelf in the south and in the Gulf of Maine in the north, the observed SST is lower than the model SST by a few degrees. With the smoothed COADS data on a $2° \times 2°$ grid one cannot expect realistic cooling in the shallow areas of the model. However, the model produces a tongue of warm water from the Florida Straits to Cape Hatteras, which is in good agreement with the observed SST. In the winter and spring, the area northeast of Cape Hatteras is somewhat warmer in the model than the observations, an indication of the mechanism of heat transfer by eddies as discussed before. The observed spring climatology indicates more northward separation than other seasons, in agreement with the model climatology. During the summer, the larger temperature gradients are observed much farther north of the Gulf Stream, which makes it difficult to identify the Gulf Stream path from surface temperature. Cornillon and Watts (1987) discuss this problem.

In Fig. 15, we plot the seasonal surface temperature from COADS. It is fairly obvious that the model SST resembles the satellite SST much better than it does the smoothed COADS SST. The difference between the model heat flux (Fig. 8) and the COADS heat flux (Fig. 2) is due to the difference in the model SST and the COADS SST through Eq. (1).

To evaluate the model in the deep ocean, we compare the area-averaged temperature profiles for each season with the average observed profiles (calculated from the seasonal climatologies of Kantha et al. 1986) in Fig. 16. In the deep ocean, the difference between the model and the observed climatologies are smaller than 0.1°C in all seasons. At the surface, the model temperature is larger by about 1°C than the observed temperature in the winter, but almost the same as the observed temperature in the other seasons. Again, it is demonstrated that more winter cooling is needed. Cold air masses advected from the continent during winter can strongly affect the air–sea interaction, but cannot be simulated if atmospheric climatological data are used. As a result, the main thermocline in the model is also warmer by ~1°C in all seasons.

We now discuss the seasonal variations in the Gulf

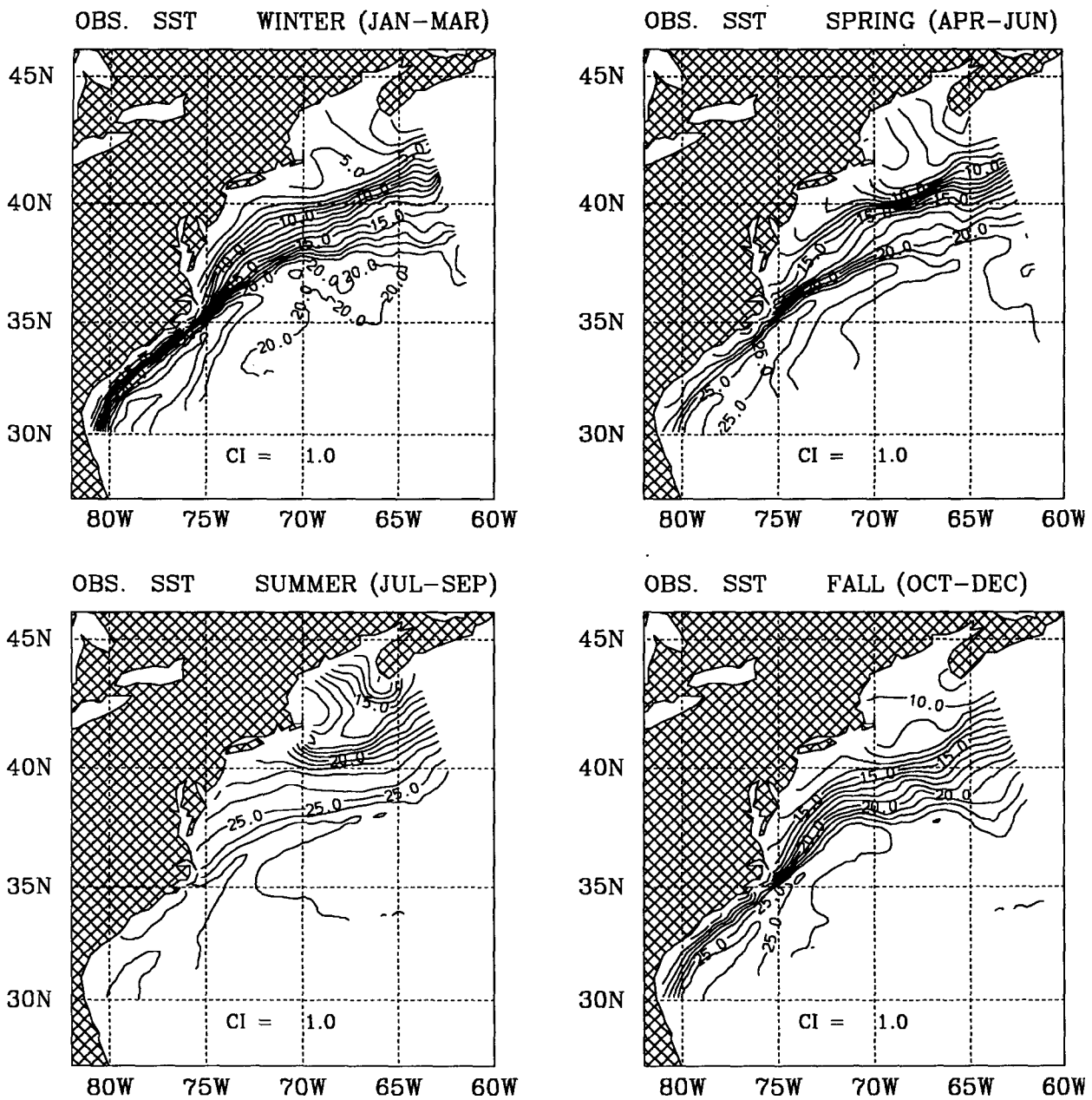

FIG. 13. Seasonal climatology of sea surface temperature obtained from the satellite-derived MCSST data. Contour interval is 1°C.

Stream path and transport as simulated by the model in experiment 6. Figure 17 shows the total streamfunction averaged over each season. Differences are evident in the circulation of each season. The northern recirculation gyre seems to be divided into two subgyres, centered around 70° and 65°N; the intensity of these subgyres changes seasonally. These subgyres intensify during the spring, when surface cooling is relatively large, widening the recirculation zone and pushing the Gulf Stream farther south. During fall and winter, the recirculation zone narrows, the Gulf Stream moves northward, and its transport decreases. This experiment suggests that the Gulf Stream transport can change considerably from one cross section to another, and from one season to another, due to local intensification of the recirculation. This could explain some of the discrepancies between the different estimates of the Gulf Stream transport. For example, Richardson (1985) references different estimates of the Gulf Stream transport that range from ~70 to ~200 Sv. When we discuss the Gulf Stream transport calculated by the model, we should keep in mind that because of the

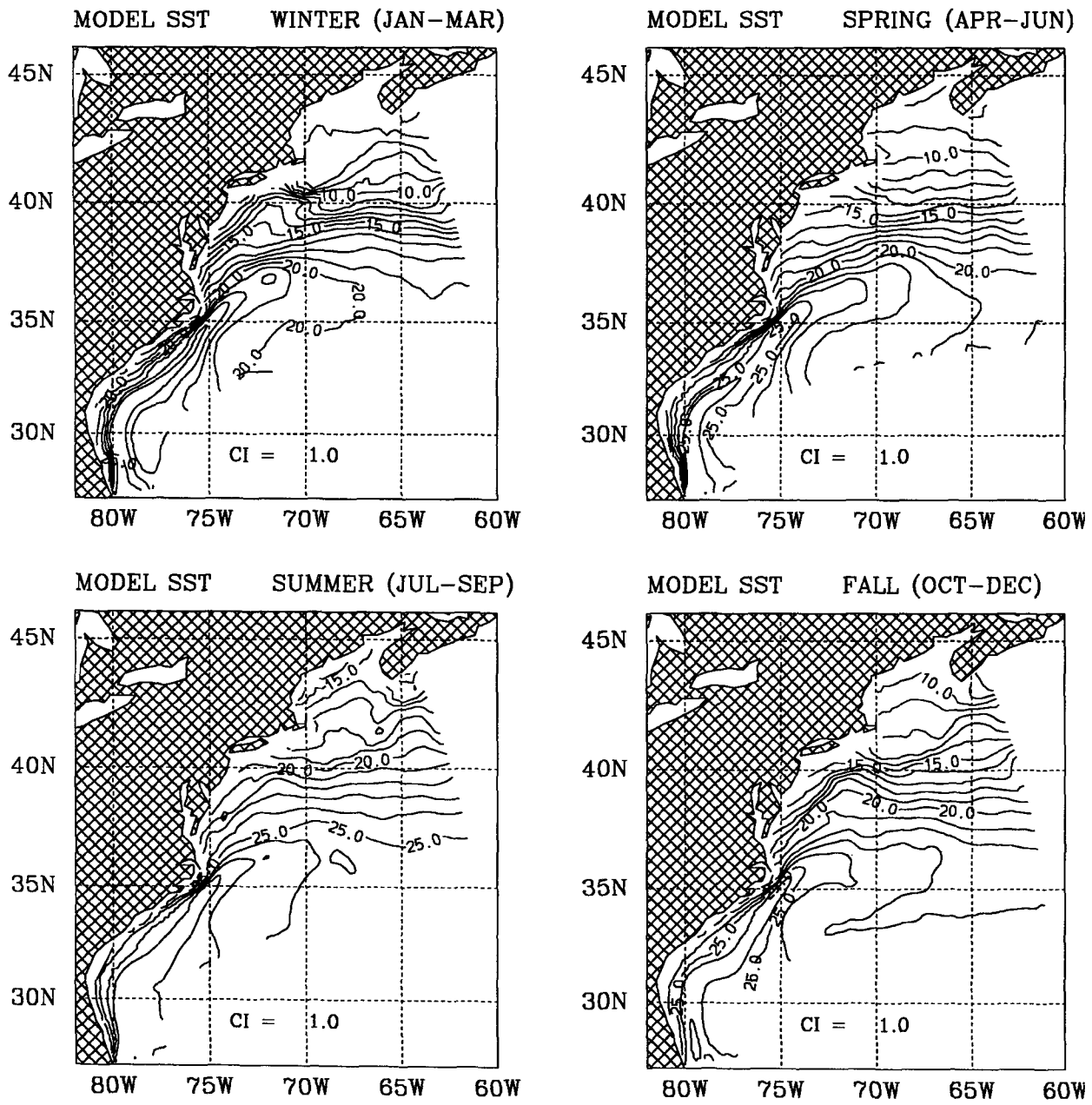

FIG. 14. As in Fig. 13 but for the seasonal climatology obtained from the model (experiment 6).

imposed boundary conditions, the Gulf Stream transport is fixed with 60 Sv entering at Cape Hatteras and 100 Sv leaving the eastern boundary. In between, changes are due to the time-dependent forcing and the thermodynamics. The increase in transport between Cape Hatteras and 62°W includes some of the 40 Sv of the slope-water inflow that joins the Gulf Stream (the other part crosses under the stream as DWBC), and local subgyre recirculation. Spatial variations in the transport are ~70 Sv, and seasonal variations are ~20 Sv. The latter number agrees with Worthington (1976), who estimated the seasonal variations as ~30 Sv.

Altimetry data indicates largest sea level differences during the springtime and smallest during fall (Fu et al. 1987). The 15-cm peak-to-peak amplitude of the sea level difference across the Gulf Stream, as calculated by Fu et al. (1987), corresponds roughly to about 5 cm s^{-1} amplitude in surface velocity. We find somewhat larger, about 10–20 cm s^{-1}, seasonal amplitude in surface velocity. As suggested by many studies before, both thermal (through surface heat flux) and me-

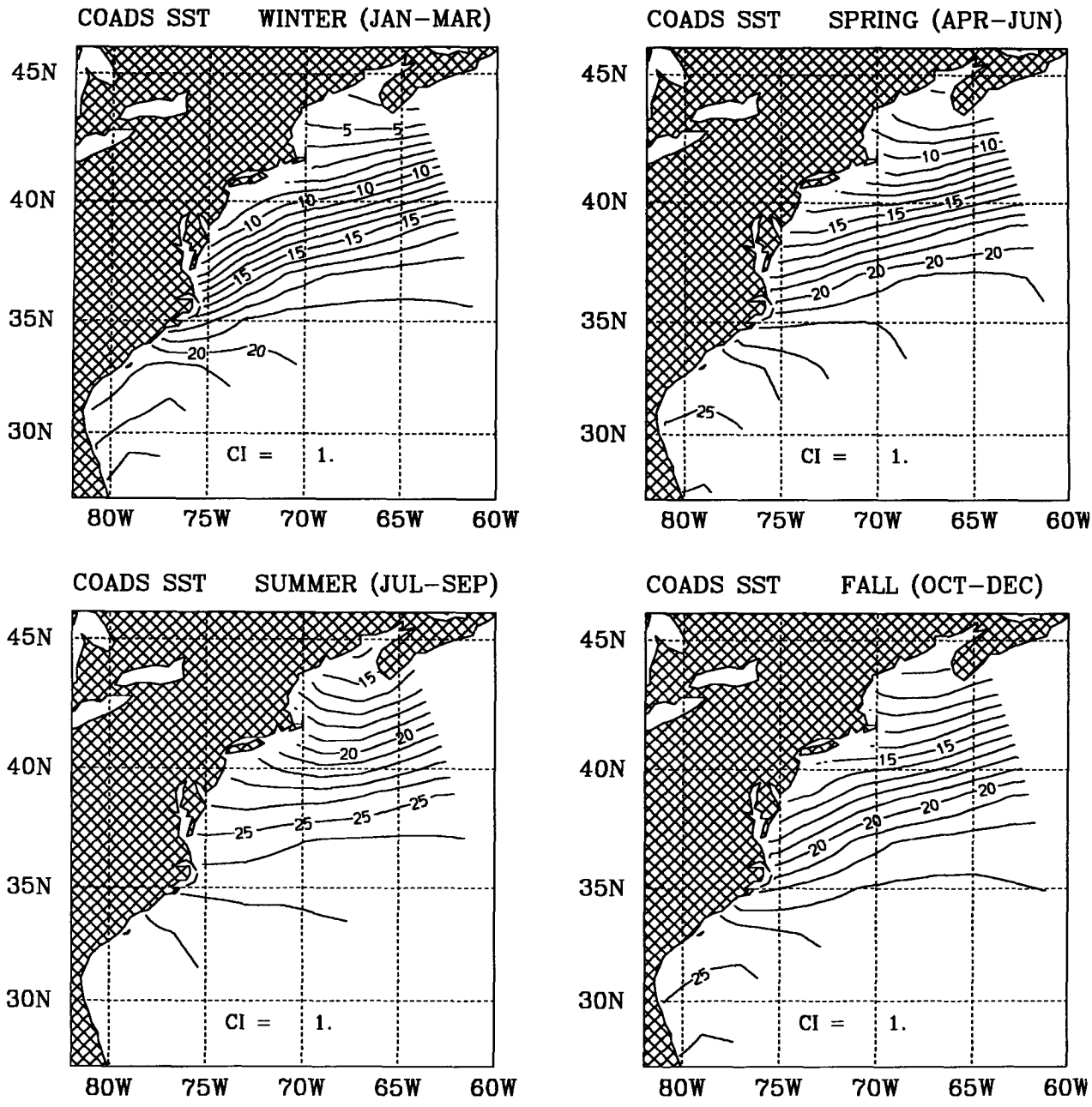

FIG. 15. As in Fig. 13 but for the seasonal climatology obtained from the COADS.

chanical (through wind stress) mechanisms are responsible for the seasonal variations of the Gulf Stream. Thus, the present study suggests that it is possible to simulate these variations with a regional eddy-resolving model that has realistic thermodynamics and mixing, even when the seasonal variation of transport on the boundaries is neglected.

7. Discussion and conclusions

In numerical simulations, the Gulf Stream tends to separate north of the observed location (Thompson and Schmitz 1989; Bryan and Holland 1989). To understand the factors governing Gulf Stream separation we have, in this paper, eliminated much of the natural variability of the system by obtaining 5-year averages; the (smoothed) location of the Gulf Stream is determined by the streamfunction representing the vertically averaged flow and the surface elevation, the gradients of which represent the surface geostrophic velocities. Overall, as the boundary conditions become more realistic, so does the resultant Gulf Stream location. Thus, experiment 6 is most in accord with the expected

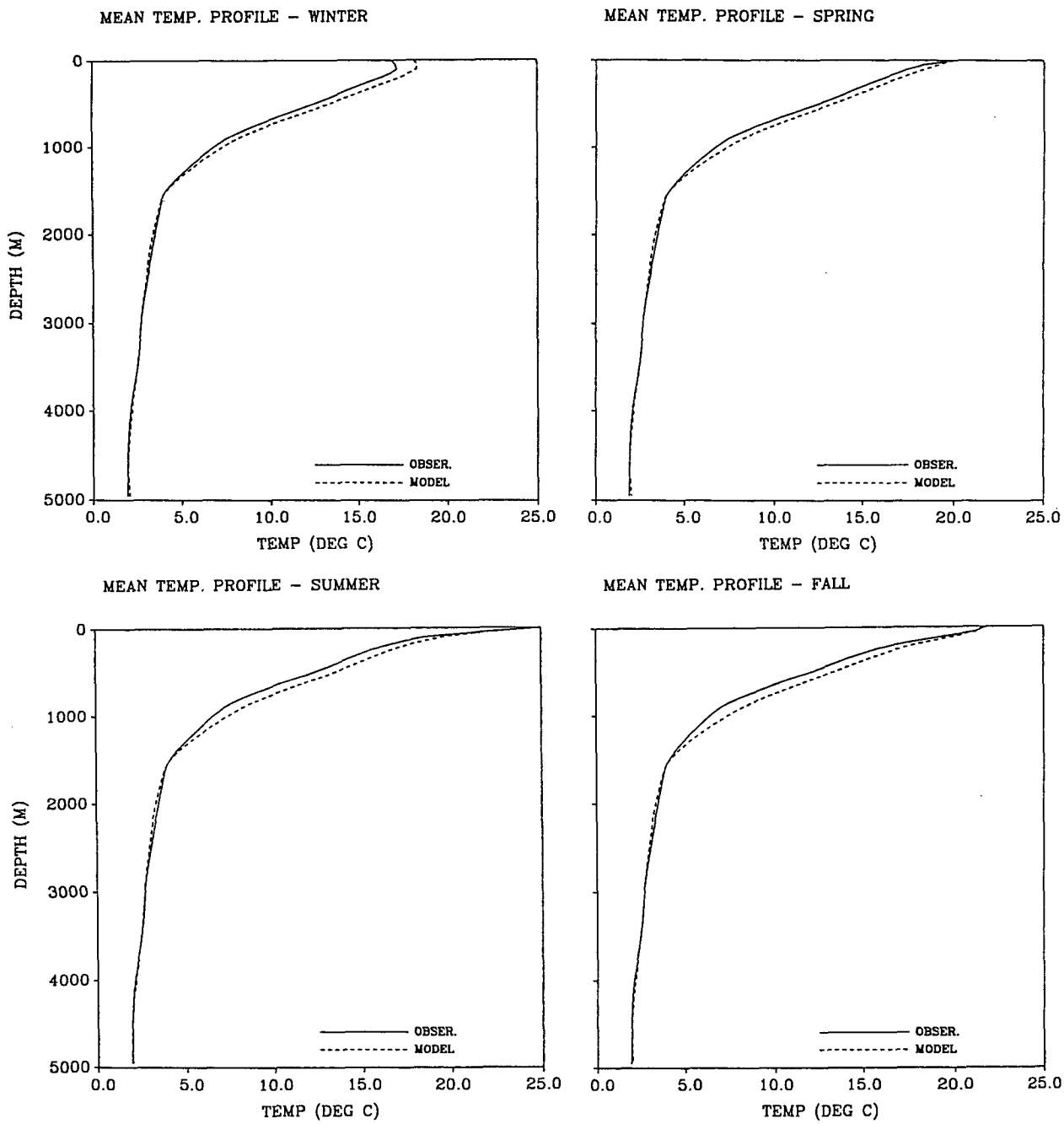

FIG. 16. Area-averaged (for regions where depth is greater than 1000 m) vertical temperature profiles of the seasonal climatologies. Solid and dashed lines represent the observed and the model climatologies, respectively.

stream location, and, for example, is in good agreement with the dynamic height calculations of Levitus (1990) and the diagnostic and geostrophic streamfunction and surface elevation calculation of Mellor et al. (1982). The latter calculation included the effects of topography, surface wind stress, and the density fields obtained from the Levitus (1982) dataset.

This paper was organized so that sensitivity calculations relative to surface forcing were first presented, followed by calculations where the lateral boundary conditions were varied. To understand the elements governing separation, let us now consider either experiments 3 or 4, shown in Fig. 7, as the standard against which to compare the other experiments: we

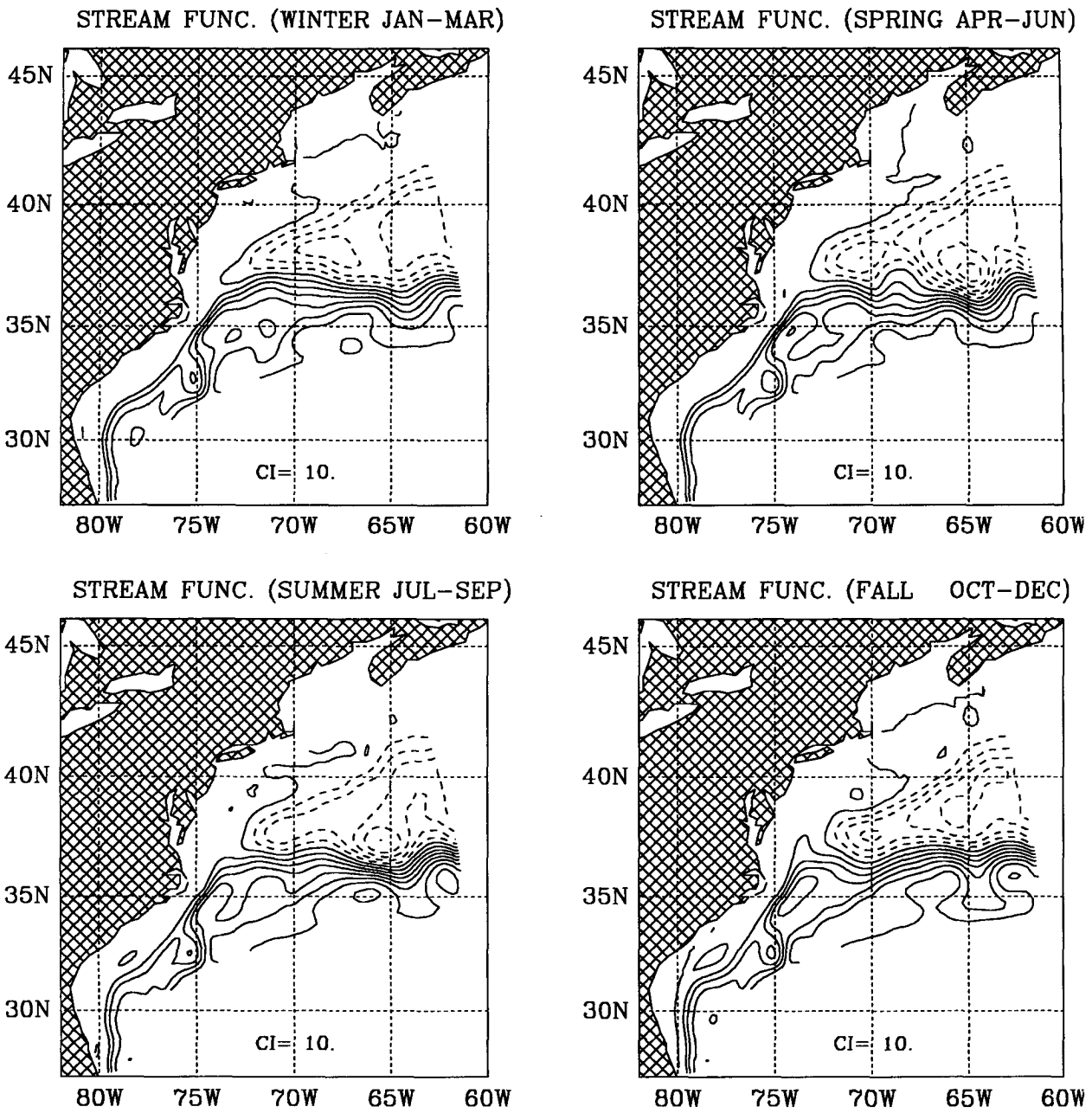

FIG. 17. Seasonal total streamfunction of experiment 6. Contour interval is 10 Sv.

ignore the relatively small difference in streamfunction and surface elevation due to seasonal versus monthly surface forcing.

First we observe that, if the slope-water inflow is removed as in experiment 5 and shown in the top panels of Fig. 12, then the model Gulf Stream continues past Cape Hatteras and climatologically separates in a diffuse manner farther to the north. Thus, the existence of the slope-water gyre consisting of a cyclonic transport of 30 to 40 Sv is necessary to the maintenance of model Gulf Stream separation at Hatteras. We expect that ageostrophic inertial effects together with local topography play a role, but these elements have not been identified explicitly in this paper. Note that Thompson and Schmitz (1989) imposed "western boundary current" inflow and outflow lateral boundary conditions on the bottom layer of their two-layer model and suggested that southward drag induced by that layer on the upper layer was a process that retarded northward migration of the Gulf Stream. Some portion

of that process may prevail here although the convenient separation of interacting layers is conceptually more difficult in the present model and in the real ocean. Furthermore, our slope current gyre is an approximately barotropic flow (Mellor et al. 1982; Richardson 1985; Hogg et al. 1986). At Hatteras the lower portion does flow under the stream and is the western boundary undercurrent (which is not visible in the total streamfunction plots; see, however, Mellor and Ezer 1991), whereas the upper portion is entrained in the Gulf Stream and plays an essential role in defining the north wall, the narrow region of strong thermal and density contrast between the slope current gyre and the Gulf Stream.

Now, in experiment 1, we removed the heat flux. In the first year, the flow, on average, is much like that in the standard experiments, 3 and 4. Then, warm-core eddies begin to transfer heat into the recirculation gyre and then sometime into the second year, the region north of the Gulf Stream warms. Simultaneously, the geostrophic velocity field moves north; thereafter, the stream flows along the shelf break north of Hatteras, after which it does separate at an unrealistically northward location. In contrast, in experiments 3 and 4, the warm eddies were cooled through the surface, particularly in the winter months, and the inflow slope current was able to maintain cooler temperatures and higher densities in the recirculating, slope-water gyre.

In comparing the standard experiments with experiment 2, which appears to be remarkably like experiment 1, we surmise that familiar mechanisms are at work in the former case; namely, southward Ekman transport, which inhibits northward meander and eddy intrusions, and the wind stress curl field, which reinforces the overall structure of the recirculation gyre.

Thus, our view of the maintenance of separation at Cape Hatteras is primarily thermodynamic; so long as the initial observed density fields are maintained, so are the resulting velocity fields. We note that theories of Gulf Stream separation often involve potential vorticity conservation. Plots of potential vorticity in, say, experiment 6 show that potential vorticity does indeed track the Gulf Stream, but, in our view, do not explain maintenance of these tracks.

Although, in these experiments, the imposed lateral inflow/outflow, vertically mean velocity boundary conditions were held fixed at the annual observed flows, time-dependent surface heat flux and wind stress were sufficiently realistic to produce some of the observed (e.g., Worthington 1976; Fu et al. 1987) seasonal variations of the Gulf Stream. For instance, seasonal variations of about 20 Sv in total transport and 10 to 20 cm s^{-1} in surface velocity were calculated. During spring, the Gulf Stream seems to be the most energetic, and during fall it is the least energetic.

Although the model has many realistic characteristics, such as bottom topography including the continental shelf, a turbulence closure scheme, thermohaline dynamics, and surface heat fluxes, the comparison between model and observed climatologies reveals some deficiencies. The model domain should be extended farther east; we see an unrealistic decrease in the variability near the open eastern boundary. Higher-resolution atmospheric forcing is needed. For example, the coarse-resolution, surface heat flux, and wind stress do not provide for sufficient winter cooling or summer heating in nearshore regions. (To add further realism to the present model, freshwater river runoff and surface salt fluxes have been added in more recent experiments. These changes affect the salinity structure on the shelf but are not important to the structure of the slope-water gyre and the Gulf Stream.) Overall, however, model calculations do seem rather realistic, and one should expect more realism in the future with improved resolution and forcing.

Acknowledgments. We thank D-S Ko and Z. Sirkes for providing the SST and the Geosat data. The support of the Institute for Naval Oceanography, the National Ocean Service, and NOAA's Geophysical Fluid Dynamics Laboratory are gratefully acknowledged. Help and advice in the development of the model were obtained from H. J. Herring, R. Patchen, and L. Kantha.

REFERENCES

Auer, S. J., 1987: Five-year climatological survey of the Gulf Stream system and its associated rings. *J. Geophys. Res.*, **92,** 11 709–11 726.

Bane, J. M., 1983: Initial observations of the subsurface structure and short-term variability of the seaward deflection of the Gulf Stream off Charleston, South Carolina. *J. Geophys. Res.*, **88,** 4673–4684.

Blumberg, A. F., and G. L. Mellor, 1983: Diagnostic and prognostic numerical circulation studies of the South Atlantic Bight. *J. Geophys. Res.*, **88,** 4579–4592.

——, and ——, 1985: A simulation of the circulation in the Gulf of Mexico. *Isr. J. Earth Sci.*, **34,** 122–144.

——, and ——, 1987: A description of a three-dimensional coastal ocean circulation model. *Three-Dimensional Coastal Ocean Models,* No. 4, N. Heaps, Ed., Amer. Geophys. Union, 208 pp.

Bryan, F., and W. R. Holland, 1989: A high-resolution simulation of the wind and thermohaline-driven circulation of the North Atlantic Ocean. *'Aha Huliko'a, Proc. of the Hawaiian Winter Workshop,* University of Hawaii, 99–116.

Cornillon, P., and D. R. Watts, 1987: Satellite thermal infrared and inverted echo sounder determination of the Gulf Stream northern edge. *J. Atmos. Oceanic Technol.*, **4,** 712–723.

Cushman-Roisin, B., 1987: On the role of heat flux in the Gulf Stream–Sargasso Sea subtropical gyre system. *J. Phys. Oceanogr.*, **17,** 2189–2202.

Ezer, T., and G. L. Weatherly, 1991: Small-scale spatial structure and long-term variability of near bottom layers in the HEBBLE area. *Deep Ocean Sediment Transport,* A. R. M. Nowell, Ed., *Mar. Geol.*, **99,** 319–328.

Fu, L-L., J. Vazquez, and M. E., Parke, 1987: Seasonal variability of the Gulf Stream from satellite altimetry. *J. Geophys. Res.*, **92,** 749–754.

Galperin, B., and G. L. Mellor, 1990a: A time-dependent, three-dimensional model of the Delaware Bay and River. Part 1: De-

scription of the model and tidal analysis. *Estuar. Coastal Shelf Sci.*, **31,** 231–253.

——, and ——, 1990b: A time-dependent, three-dimensional model of the Delaware Bay and River. Part 2: Three-dimensional flow fields and residual circulation. *Estuar. Coastal Shelf Sci.*, **31,** 255–281.

Garratt, J. R., 1977: Review of drag coefficients over oceans and continents. *Mon. Wea. Rev.*, **105,** 915–929.

Grossman, R. L., and A. K. Betts, 1990: Air–sea interaction during an extreme cold air outbreak from the eastern coast of the United States. *Mon. Wea. Rev.*, **118,** 324–342.

Hellerman, S., and M. Rosenstein, 1983: Normal monthly wind stress over the world ocean with error estimates. *J. Phys. Oceanogr.*, **13,** 1093–1104.

Hogg, N. G., R. S. Pickart, R. M. Hendry, and W. J. Smethie, 1986: The northern recirculation gyre of the Gulf Stream. *Deep-Sea Res.*, **33,** 1139–1165.

Holland, W. R., and W. J. Schmitz, 1985: Zonal penetration scale of midlatitude jets. *J. Phys. Oceanogr.*, **15,** 1859–1875.

Ionov, V. V., G. L. Weatherly, and R. Harkema, 1986: On the temporal variability of the surface Gulf Stream and near-bottom flows. *J. Geophys. Res.*, **91,** 2661–2666.

Jerlov, N. G., 1976: *Marine Optics.* Elsevier, 231 pp.

Kantha, L. H., H. J. Herring, and G. L. Mellor, 1986: South Atlantic Bight OCS circulation model. Dynalysis of Princeton, Report No. 91, 154 pp.

Kondo, J., 1975: Air–sea bulk transfer coefficients in diabatic conditions. *Bound.-Layer Meteor.*, **9,** 91–112.

Leaman, K. D., R. L. Molinari, and P. S. Vertes, 1987: Structure and variability of the Florida Current at 27°N: April 1982–July 1984. *J. Phys. Oceanogr.*, **17,** 565–583.

Levitus, S., 1982: *Climatological Atlas of the World Ocean.* U.S. Dept. of Commerce and NOAA, 173 pp.

——, 1990: Interpentadal variability of steric sea level and geopotential thickness of the North Atlantic Ocean, 1970–1974 versus 1955–1959. *J. Geophys. Res.*, **95,** 5233–5238.

Luyten, J. R., J. Pedlosky, and H. Stommel, 1983: The ventilated thermocline. *J. Phys. Oceanogr.*, **13,** 292–309.

Mellor, G. L., 1991: An equation of state for numerical models of ocean and estuaries. *J. Atmos. Oceanic Technol.*, **8,** 609–611.

——, and T. Yamada, 1982: Development of a turbulence closure model for geophysical fluid problems. *Rev. Geophys. Space Phys.*, **20,** 851–875.

——, and A. F. Blumberg, 1985: Modeling vertical and horizontal diffusivities with the sigma coordinate system. *Mon. Weather Rev.*, **113,** 1279–1383.

——, and T. Ezer, 1991: A Gulf Stream model and an altimetry assimilation scheme. *J. Geophys. Res.*, **96,** 8779–8795.

——, C. Mechoso, and E. Keto, 1982: A diagnostic calculation of the general circulation of the Atlantic Ocean. *Deep-Sea Res.*, **29,** 1171–1192.

Niiler, P. P., and W. S. Richardson, 1973: Seasonal variability of the Florida Current. *J. Mar. Res.*, **31,** 144–167.

Nof, D., 1983: On the response of ocean currents to atmospheric cooling. *Tellus*, **35A,** 60–72.

Nurser, A. J. G., and R. G. Williams, 1990: Cooling Parsons' model of the separated Gulf Stream. *J. Phys. Oceanogr.*, **20,** 1974–1979.

Oberhuber, J. M., 1988: An atlas based on the COADS data set: the budgets of heat, buoyancy and turbulent kinetic energy at the surface of the global ocean. Max-Planck Institüt für Meteorologie, Rep. No. 15.

Oey, L-Y., G. L. Mellor, and R. I. Hires, 1985a: A three-dimensional simulation of the Hudson-Raritan estuary. Part I: Description of the model and model simulations. *J. Phys. Oceanogr.*, **15,** 1676–1692.

——, ——, and ——, 1985b: A three-dimensional simulation of the Hudson–Raritan estuary. Part II: Comparison with observation. *J. Phys. Oceanogr.*, **15,** 1693–1709.

Olson, D. B., O. B. Brown, and S. R. Emmerson, 1983: Gulf Stream frontal statistics from Florida Straits to Cape Hatteras derived from satellite and historical data. *J. Geophys. Res.*, **88,** 4569–4577.

Richardson, P. L., 1983: Eddy kinetic energy in the North Atlantic from surface drifters. *J. Geophys. Res.*, **88,** 4355–4367.

——, 1985: Average velocity and transport of the Gulf Stream near 55°W. *J. Mar. Res.*, **43,** 83–111.

Robinson, A. R., M. A. Spall, and N. Pinardi, 1988: Gulf Stream simulations and the dynamics of ring and meander processes. *J. Phys. Oceanogr.*, **18,** 1811–1853.

Spall, M. A., and A. R. Robinson, 1990: Regional primitive equation studies of the Gulf Stream meander and ring formation region. *J. Phys. Oceanogr.*, **20,** 985–1016.

Schott, F. A., T. N. Lee, and R. Zantopp, 1988: Variability of structure and transport of the Florida Current in the period range of days to seasonal. *J. Phys. Oceanogr.*, **18,** 1209–1230.

Thompson, J. D., and W. J. Schmitz, 1989: A limited-area model of the Gulf Stream: Design, initial experiments, and model–data intercomparison. *J. Phys. Oceanogr.*, **19,** 791–814.

Trenberth, K. E., W. G. Large, and J. G. Olson, 1990: The mean annual cycle in global ocean wind stress. *J. Phys. Oceanogr.*, **20,** 1742–1760.

Veronis, G., 1981: Dynamics of large-scale ocean circulation. *Evolution of Physical Oceanography,* B. A. Warren and C. Wunsch, Eds., The MIT Press, 157 pp.

Worthington, L. V., 1962: Evidence for a two gyre circulation in the North Atlantic. *Deep-Sea Res.*, **9,** 51–67.

——, 1976: *On the North Atlantic Circulation.* Johns Hopkins University Press, 110 pp.

Wright, P. B., 1988: An atlas based on the COADS data set: Fields of mean wind, cloudiness and humidity at the surface of the global ocean. Max-Planck Institüt für Meteorologie, Rep. No. 14.

Zheng Q., V. Klemas, and N. E. Huang, 1984: Dynamics of the slope water off New England and its influence on the Gulf Stream as inferred from satellite IR data. *Remote Sens. Environ.*, **15,** 135–153.